

Buffon-Laplace Needle Problem as a geometric probabilistic approach to filtration process

Yan-Jie Min,^{*} De-Quan Zhu,^{*} and Jin-Hua Zhao[†]
*CoCoLab, School of Data Science and Engineering,
South China Normal University, Shanwei 516622, China*
(Dated: December 2, 2024)

Buffon-Laplace Needle Problem considers a needle of a length l randomly dropped on a large plane distributed with vertically parallel lines with distances a and b ($a \geq b$), respectively. As a classical problem in stochastic probability, it serves as a mathematical basis of various physical literature, such as the efficiency of a filter and the emergence of clogging in filtration process. Yet its potential application is limited by previous focus on its original form of the ‘short’ needle case of $l < b$ and its analytical difficulty in a general sense. Here, rather than a ‘short’ needle embedded in two-dimensional space, we analytically solve problem versions with needles and spherocylinders of arbitrary length and radius embedded in two- and three-dimensional spaces dropped on a grid with any rectangular shape. We further confirm our analytical theory with Monte Carlo simulation. Our framework here helps to provide a geometric analytical perspective to filtration process, and also extend the analytical power of the needle problem into unexplored parameter regions for physical problems involving stochastic processes.

arXiv:2402.06670v4 [math.HO] 28 Nov 2024

^{*} These authors contributed equally to this work.

[†] zhaojh@m.scnu.edu.cn

I. INTRODUCTION

Filtration process of particles through a filter or a porous medium is a fundamental subject in soft and granular matter research [1, 2]. Theoretical methods are developed to characterize its static and dynamical properties, such as the efficiency of a filter and the onset of clogging [3–7]. Some methods explore the geometry of particles and filters to construct probabilistic models. In the paper [5], a filtration process of particles is considered in two parts: (1) individual particles in a flow arrive at and make contact with a mesh structure, and (2) the interaction between the particles and the mesh after contacts leads to a formation of an arch of particles and results in clogging. Following this logic, the paper [8] considers particles as rod-like objects and adopts a generalized version of the Buffon-Laplace Needle Problem (BLNP) as a geometric probabilistic approach to the above first part. In this paper, we follow the paper [8] and focus on the analytical result of BLNP for filtration process.

BLNP [9, 10] is one of the oldest problems in geometric probability dated back more than two centuries. BLNP considers randomly dropping a thin needle (i.e. a line segment) with a length l on a two-dimensional (2D) plane distributed with two sets of equidistant parallel lines with distances a and b , respectively, which are vertical to each other, and studies the statistical property of intersections between the needle and the lines. For convenience, we set $a \geq b$ in this paper. BLNP is a natural extension of Buffon’s Needle Problem (BNP) [11], which considers a similar setting on a plane yet with a single set of parallel lines with a distance d .

For the two needle problems, except the filtration process of particles, there are other contexts in which the scenario of needle dropping is also involved, such as random sequential adsorption which considers dropping line segments and other geometrical shapes in a non-overlapping way onto a substrate to study its jamming property [12–15], and random-line graphs which are formed by intersections by line segments dropped in a square on a plane [16].

The fundamental quantity for the two needle problems is the intersection probability of a needle intersecting with at least one line. For the intersection probability $P(l, d)$ with a needle length l and a line distance d in BNP, [11] and [17](page 251-252) derive its form for the ‘short’ needle case with $l < d$. [17](page 258, problem 7) also shows $P(l, d)$ for a long needle case with $l > d$. For the intersection probability $P(l, a, b)$ with a needle length l and line distances a and b in BLNP, [9, 10] and [17](page 255-257) show a prediction of the case with $l < b$. In [8], the authors further lay down an analytical form of $P(l, a, b)$ in a specific case of $a = b$ and $l > b$ (as Eq. (6) in its main text), yet with an error in a coefficient which we will show later. Another quantity pertinent to the two needle problems is the statistics of numbers of intersections and visited grids for a long needle. For BNP, [18] shows the distribution of intersection numbers in the case of $l > d$. For BLNP, [19] studies the average and the maximal number of visited grids (tiles) for a needle on any rectangular grid.

As classical models of randomness, variants based on BNP and BLNP are frequently discussed in both mathematical and physical literature. A simple variation of the problems is to generalize needles and grid lines into other geometrical objects. For BNP, a needle can be replaced with a planar curve [20, 21], polygons [22], a pivot needle (two needles sharing a tip) [23], and so on. Sets of parallel lines can also be generalized to parallel stripes with a finite width [24], random Cantor sets [25, 26], a line with randomly distributed dots [27], and so on. For BLNP, a needle can be extended to an ellipse [28], a spherocylinder (a rod-like shape consistent of a cylinder and two hemispherical caps on both its ends) in three-dimensional (3D) space [8, 29], and so on. Besides, a plane in BLNP can be considered as being covered with congruent triangles [17] (page 258, problem 8).

In this paper, we revisit BLNP and focus on its analytical solution of intersection probability, the most basic quantity of the problem. For the original BLNP and its extensions, the initial ‘short’ needle case with $l < b$ is heavily discussed in previous literature, while analytical result for the ‘long’ needle case of $l > b$ is quite limited. In the paper [8], after a needle in 2D space is generalized to a spherocylinder in 3D space, BLNP is adopted as a model for granular particles arriving at a sieve-like grid. Yet it sets $a = b$ for a square mesh, and lays down the intersection probability in the initial form of integrals and estimates the probability with Monte Carlo simulation [30]. Here we emphasize that, neither forcing $l < b$ nor $a = b$ is necessary for a theoretical model, and models with any permissible l and (a, b) represents a realistic setting when the problem serves as an approximation model in a physical context.

Our main contribution in this paper is that, with a single geometric probabilistic framework, we solve BLNP with dropped objects as needles with no volume and spherocylinders with finite volume in both 2D and 3D spaces, and derive analytical predictions of intersection probability for any shape parameter (a length l for a needle and a length l and a radius $\sigma/2$ for a spherocylinder) and any grid shape parameters (a, b) . Our results theoretically elucidate the contact probability between spherocylinders in flow in 3D space with a mesh for the model presented in [8], and makes possible studying new complex phenomena originated from long particles and irregular grid topology. Our theory helps to construct a full geometric probabilistic picture of the filtration process further combined with the interaction between particles and mesh. Besides, on the mathematical side, our framework naturally retrieves the result for the original BLNP with ‘short’ needles. In all, our framework helps to release the potential of BLNP as a mathematical basis in various physical problems.

Here is the layout of the paper. In Section II, we present BLNP and its four versions, and also lay down their

representation and realization in simulation. In Sections III to VI, we explain the analytical framework to calculate the intersection probability when needles and spherocylinders embedded in 2D and 3D spaces, respectively, are dropped on a 2D grid. In Section VII, we compare our theoretical results with previous ones. In Section VIII, we show our theoretical results, verified with Monte Carlo simulation. In Section IX, we conclude the paper with some discussion. In Appendices A–J, we leave details of calculation for the analytical framework.

II. MODEL

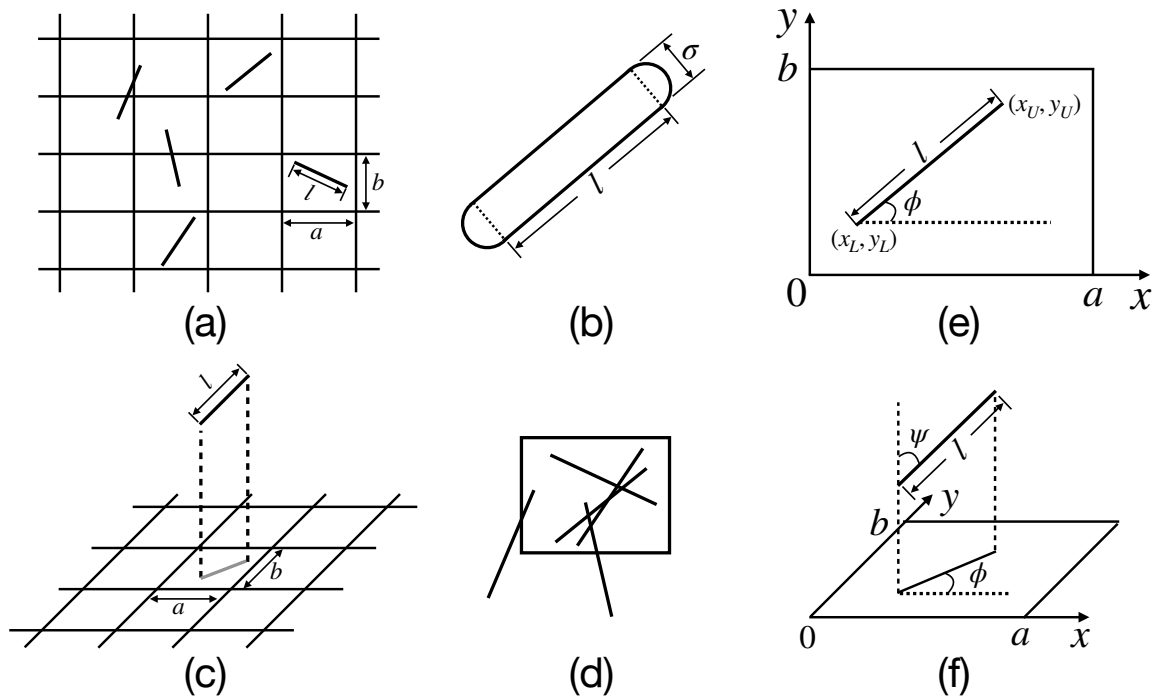


FIG. 1. BLNP with needles and spherocylinders in 2D and 3D spaces. (a) In the original BLNP with needles, a thin needle of a length l is repeatedly dropped on a plane distributed with two vertical sets of parallel lines with distances of a and b , respectively. The five line segments in the grid represent needle experiments, in two of which a needle intersects with lines. (b) A 2D needle is extended to a 2D spherocylinder, which consists of a rectangle with a width l and two semicircles with a diameter σ on both its ends. (c) A 2D needle is extended to a 3D one, in which a needle of a length l in a 3D space is dropped onto a 2D plane. A 3D needle intersects with lines only when its projection on the 2D plane intersects with them. (d) The five needle configurations in (a) are moved in a periodical way into a single grid cell, while their statuses between a needle and lines are retained respectively. (e) In the BLNP with 2D needles, the relative position of a needle within a grid cell with a width a and a height b is shown. The coordinates (x_U, y_U) and (x_L, y_L) represent respectively the upper and the lower tips of the needle, and the orientation $\phi \in [0, \pi)$ is the angle between the needle and the x -axis. (f) In the BLNP with 3D needles, a 3D needle is firstly projected onto a 2D grid. The orientation $\psi \in [0, \pi/2]$ is the angle between the needle and the direction perpendicular to the grid. The relative position of a projected needle in a grid cell shares a similar description in the case of 2D needles shown in (e).

In the original BLNP, the grid is 2D with two vertical sets of parallel lines, and a needle is dropped on the plane. See Fig.1(a) for an example. In this paper, when an object is embedded in 2D or 3D spaces, we call the type of the object as 2D or 3D one, respectively, for convenience. We keep the grid as 2D and generalize the dropped object from a 2D needle into two directions. We first generalize a thin needle with no volume into a rod-like shape with a finite volume. This generalization makes possible consideration of real-world objects in a mathematical model. A spherocylinder [8, 29] is intrinsically a 3D object, and consists of a cylinder with a length l and two semispheres with a radius $\sigma/2$ on both its ends. When such a spherocylinder lies on a plane, its 2D projection on the plane consists of a rectangle with a width l and two semicircles with a diameter σ on both its ends. We simply call this shape a 2D spherocylinder. See Fig.1(b) for an example. We then generalize the embedded space of dropped objects from 2D to 3D, during which an extra degree of freedom is introduced for the objects. See Fig.1(c) for an example of a 3D

needle. Beware that, an intersection between a 3D object and a 2D grid is defined between the projection of the 3D object onto the grid plane and the grid lines. Due to its simple topology, the projection of a 3D spherocylinder on a 2D plane is a 2D one, yet with a shorter length except when it is parallel to the plane.

Summing up the above generalizations of BLNP, we consider here its four versions: (1) BLNP with 2D needles, which is simply the original BLNP; (2) BLNP with 2D spherocylinders; (3) BLNP with 3D needles; and (4) BLNP with 3D spherocylinders.

We further lay down how to perform simulation for these four versions. To count the intersection events, it is only relevant to distinguish whether or not a dropped object intersects with sets of lines, which only involves the relative position between them. Thus the picture of an object dropped on a grid with an infinitely large number of cells can be simplified into one in which an object is dropped on a single grid cell. See Fig.1(d) for an example when all needles are moved into a single grid cell. We choose parallel lines with distances b and a to establish x - and y -axes, respectively, and then consider the relative position of a dropped object in a grid cell. As a needle and a spherocylinder both have simple geometrical boundaries, we can use only a limited number of parameters, for example coordinates of their two tips, to describe their overall positions. A general Monte Carlo simulation[30] of an object-dropping experiment can be carried out as follows: with given sizes of objects and grid cells (l, a, b) or (l, σ, a, b) , we first generate a large number N_{all} of object configurations with a pseudo-random number generator, say $\text{Rand}()$, which generates a sequence of real numbers $\in (0, 1)$ obeying a uniform distribution; we then count the number N_{coll} of configurations in which an object overlaps with at least one boundary of a grid cell; finally, we calculate the empirical intersection probability as $N_{\text{coll}}/N_{\text{all}}$.

In the above simulation process, only the description of an object configuration and the condition for an intersection vary in the four problem versions. For a 2D needle and spherocylinder, their descriptions of relative positions share a similar form and consist of three ingredients: the coordinate x_U on x -axis and the coordinate y_U on y -axis for the upper tip of a needle or the center of the upper semicircle of a spherocylinder, and the orientation ϕ between a needle or a spherocylinder and the x -axis. The ‘upper’ tip or semicircle here corresponds to the one of tips or semicircles with a larger coordinate on the y -axis. Fig.1(e) shows an illustration for the 2D needle case. The ranges of (x_U, y_U, ϕ) are $[0, a)$, $[0, b)$, and $[0, \pi)$, respectively. In a single experiment, a random configuration of a 2D needle or spherocylinder can be generated as

$$\begin{bmatrix} x_U \\ y_U \\ \phi \end{bmatrix} = \begin{bmatrix} a \times \text{Rand}() \\ b \times \text{Rand}() \\ \pi \times \text{Rand}() \end{bmatrix}. \quad (1)$$

Correspondingly, the coordinates of the lower tip of the needle or the center of the lower semicircle of the spherocylinder are

$$\begin{bmatrix} x_L \\ y_L \end{bmatrix} = \begin{bmatrix} x_U - l \cos \phi \\ y_U - l \sin \phi \end{bmatrix}. \quad (2)$$

For the description of a 3D needle or spherocylinder, except from the parameters (x_U, y_U, ϕ) , a fourth parameter $\psi \in [0, \pi/2]$ is introduced to account the orientation between an object and the axis vertical to the grid plane. Fig.1 (f) shows an illustration for the 3D needle case. To generate a random configuration of a 3D needle or spherocylinder, we have

$$\begin{bmatrix} x_U \\ y_U \\ \psi \\ \phi \end{bmatrix} = \begin{bmatrix} a \times \text{Rand}() \\ b \times \text{Rand}() \\ \frac{\pi}{2} \times \text{Rand}() \\ \pi \times \text{Rand}() \end{bmatrix}. \quad (3)$$

Correspondingly, the coordinates of the lower tip of the 3D needle or the center of the lower semicircle of the 3D spherocylinder of their projected shapes are respectively

$$\begin{bmatrix} x_L \\ y_L \end{bmatrix} = \begin{bmatrix} x_U - l \sin \psi \cos \phi \\ y_U - l \sin \psi \sin \phi \end{bmatrix}. \quad (4)$$

Then we consider the condition for an intersection between a dropped object and a grid cell. An intersection between a 2D needle and the grid happens simply when at least one tip is out of the grid cell. We can state as

$$\begin{aligned} & (x_L < 0) \vee (a < x_L) \\ & \vee (y_L < 0) \vee (b < y_L), \end{aligned} \quad (5)$$

in which \vee is a logical OR operator. Beware that, in the numerical simulation with continuous real numbers, we ignore the cases when the two needle tips fall exactly on any boundary of a grid cell (say, $x = 0$ and a , and $y = 0$ and b), since their probability is infinitesimal.

To account an intersection between a 2D spherocylinder, also the 2D projection of a 3D spherocylinder, and a grid cell, the contour of a spherocylinder should be taken into consideration. It is easy to find that, an intersection happens when at least one of the furthestmost tips in four directions of the contour of a spherocylinder is out of a grid cell. We have the following condition as

$$\begin{aligned} & \left(x_U - \frac{\sigma}{2} < 0\right) \vee \left(a < x_U + \frac{\sigma}{2}\right) \\ & \vee \left(y_U - \frac{\sigma}{2} < 0\right) \vee \left(b < y_U + \frac{\sigma}{2}\right) \\ & \vee \left(x_L - \frac{\sigma}{2} < 0\right) \vee \left(a < x_L + \frac{\sigma}{2}\right) \\ & \vee \left(y_L - \frac{\sigma}{2} < 0\right) \vee \left(b < y_L + \frac{\sigma}{2}\right). \end{aligned} \tag{6}$$

When the line distance $a \rightarrow \infty$, the constraint from parallel lines along the y -axis vanishes, and two sets of parallel lines effectively reduce to only one set. In this case, the BLNP with 2D needles, 2D spherocylinders, 3D needles, and 3D spherocylinders reduce to its BNP versions, respectively. For the simulation of four BNP versions, we can simply remove x_U and x_L from the description of object configuration in Eqs.(1)-(4), along with those terms with x_U and x_L in Eqs.(5) and (6).

Based on the above representations of the relative position of an object dropped on a grid, we further develop a consistent analytical framework to calculate the intersection probability with any size of objects and grid cells. In the following four sections, starting from the original BLNP version with 2D needles, we theoretically solve problems with increasing complexity until the one with 3D spherocylinders. Furthermore, by setting $1/a \rightarrow 0$, these theoretical equations naturally reduce to those for the four BNP versions, respectively.

III. THEORY OF BLNP WITH 2D NEEDLES

To compute the intersection probability for the four BLNP versions, our basic logic is to navigate in the parameter space of configurations of a dropped object in a grid cell and calculate the fraction of the volume of parameter space, in which an intersection happens, among the total volume of the parameter space.

Specifically, for the BLNP with 2D needles, we calculate two volumes: S_{all} as one of the total parameter space of (x_U, y_U, ϕ) for a needle configuration, and S_{coll} as one of the proper parameter space of (x_U, y_U, ϕ) which results in an intersection between the needle and the grid cell. The intersection probability $P(l, a, b)$ can be formulated as

$$P(l, a, b) = \frac{S_{\text{coll}}}{S_{\text{all}}}. \tag{7}$$

It is easy to find that

$$S_{\text{all}} = ab\pi. \tag{8}$$

The challenging part here is to derive an explicit form for S_{coll} . We reformulate S_{coll} as

$$S_{\text{coll}} = S_{\text{coll}}(x) + S_{\text{coll}}(y) - S_{\text{coll}}(x, y), \tag{9}$$

in which $S_{\text{coll}}(x)$, $S_{\text{coll}}(y)$, and $S_{\text{coll}}(x, y)$ denote the volume of the parameter space of (x_U, y_U, ϕ) when an intersection between a 2D needle and a grid cell happens on the boundaries of the grid cell along the y -axis (say, $x = 0$ and a), the x -axis (say, $y = 0$ and b), and the x - and y -axes at the same time, respectively. In the following equations, we

denote (x, y) for (x_U, y_U) for convenience. Based on Eqs.(1), (2), and (5), we have

$$\begin{aligned} S_{\text{coll}}(x) &= \int_0^{\frac{\pi}{2}} d\phi \int_0^a \Theta(l \cos \phi - x) dx \int_0^b dy + \int_{\frac{\pi}{2}}^{\pi} d\phi \int_0^a \Theta(-l \cos \phi + x - a) dx \int_0^b dy \\ &= b \int_0^{\pi} d\phi \int_0^a \Theta(|l \cos \phi| - x) dx, \end{aligned} \quad (10)$$

$$\begin{aligned} S_{\text{coll}}(y) &= \int_0^{\pi} d\phi \int_0^a dx \int_0^b \Theta(l \sin \phi - y) dy \\ &= a \int_0^{\pi} d\phi \int_0^b \Theta(l \sin \phi - y) dy, \end{aligned} \quad (11)$$

$$\begin{aligned} S_{\text{coll}}(x, y) &= \int_0^{\frac{\pi}{2}} d\phi \int_0^a \Theta(l \cos \phi - x) dx \int_0^b \Theta(l \sin \phi - y) dy + \int_{\frac{\pi}{2}}^{\pi} d\phi \int_0^a \Theta(-l \cos \phi + x - a) dx \int_0^b \Theta(l \sin \phi - y) dy \\ &= \int_0^{\pi} d\phi \int_0^a \Theta(|l \cos \phi| - x) dx \int_0^b \Theta(l \sin \phi - y) dy. \end{aligned} \quad (12)$$

The step function $\Theta(x)$ is defined as $\Theta(x) = 1$ if $x \geq 0$ and 0 otherwise. Combining a step function with the integrands on the parameters (x_U, y_U, ϕ) singles out proper ranges which permit an intersection between a needle and a grid cell. On the righthand side of Eqs.(10) and (12), we make a change of variables as $x - a \rightarrow -\hat{x}$. We have

$$\begin{aligned} \int_0^a \Theta(-l \cos \phi + x - a) dx &= \int_a^0 \Theta(-l \cos \phi - \hat{x}) d(-\hat{x}) \\ &= \int_0^a \Theta(-l \cos \phi - \hat{x}) d\hat{x}. \end{aligned} \quad (13)$$

An alternative way to calculate S_{coll} is

$$S_{\text{coll}} = S_{\text{all}} - S_{\text{non-coll}}, \quad (14)$$

in which $S_{\text{non-coll}}$ is the volume of the parameter space of (x_U, y_U, ϕ) where there is no intersection between a needle and a grid cell. Following the same logic in Eqs.(10)-(12), we have

$$S_{\text{non-coll}} = \int_0^{\pi} d\phi \int_0^a \Theta(x - |l \cos \phi|) dx \int_0^b \Theta(y - l \sin \phi) dy. \quad (15)$$

We should mention that these two frameworks to calculate S_{coll} are equivalent. Yet the former is more direct in computation, which we will follow in this paper.

To calculate Eqs.(10)-(12), we first define three integrals as

$$A(l, a) \equiv \int_0^{\pi} d\phi \int_0^a \Theta(|l \cos \phi| - x) dx, \quad (16)$$

$$B(l, b) \equiv \int_0^{\pi} d\phi \int_0^b \Theta(l \sin \phi - y) dy, \quad (17)$$

$$AB(l, a, b) \equiv \int_0^{\pi} d\phi \int_0^a \Theta(|l \cos \phi| - x) dx \int_0^b \Theta(l \sin \phi - y) dy. \quad (18)$$

Correspondingly, we rewrite S_{coll} as

$$S_{\text{coll}} = bA(l, a) + aB(l, b) - AB(l, a, b). \quad (19)$$

To finish the computation of Eqs.(16)-(18) and finally $P(l, a, b)$, we should examine the relative sizes among l , a , and b . We leave details of calculation in Appendix A. With Eqs.(A.10), (A.13), (A.16), and (A.19), we lay down our final equations as

$$P(l, a, b) = \begin{cases} \frac{2}{\pi} \left(\frac{l}{a} + \frac{l}{b} \right) - \frac{1}{\pi} \frac{l^2}{ab}, & \text{if } l \leq b; \\ \frac{1}{\pi} \frac{b}{a} + \frac{2}{\pi} \frac{l}{b} \left(1 - \sqrt{1 - \frac{b^2}{l^2}} \right) + \frac{2}{\pi} \left(\frac{\pi}{2} - \arcsin \frac{b}{l} \right), & \text{if } b < l \leq a; \\ \frac{1}{\pi} \left(\frac{L^2}{ab} + \frac{l^2}{ab} \right) - \frac{2}{\pi} \left(\frac{l}{a} \sqrt{1 - \frac{a^2}{l^2}} + \frac{l}{b} \sqrt{1 - \frac{b^2}{l^2}} \right) \\ + \frac{2}{\pi} \left(\pi - \arcsin \frac{a}{l} - \arcsin \frac{b}{l} \right), & \text{if } a < l \leq L; \\ 1, & \text{if } L < l, \end{cases} \quad (20)$$

in which we define $L \equiv \sqrt{a^2 + b^2}$.

We find that when $l > L$, we have $P(l, a, b) = 1$. This result has a simple geometrical interpretation. The longest distance between two points in a grid cell with a width a and a height b is the diagonal line with a distance of L . Thus any needle with a length $l > L$ dropped on a grid is certain to intersect with grid lines, leading to $P(l, a, b) = 1$.

A necessary condition for the correctness of Eq.(20) is the consistency of $P(l, a, b)$, and equivalently S_{coll} , at the boundaries of the four cases of l . We leave details of calculation in Appendix B.

When $a \rightarrow \infty$, then $l/a \rightarrow 0$. Eq.(20) simplifies to the result for the BNP with 2D needles as

$$P(l, \infty, b) = \begin{cases} \frac{2}{\pi} \frac{l}{b}, & \text{if } l \leq b; \\ \frac{2}{\pi} \frac{l}{b} \left(1 - \sqrt{1 - \frac{b^2}{l^2}}\right) + \frac{2}{\pi} \left(\frac{\pi}{2} - \arcsin \frac{b}{l}\right), & \text{if } b < l. \end{cases} \quad (21)$$

IV. THEORY OF BLNP WITH 2D SPHEROCYLINDERS

Following the language in the BLNP with 2D needles, we calculate the intersection probability for the BLNP with 2D spherocylinders as

$$P(l, \sigma, a, b) = \frac{S_{\text{coll}}}{S_{\text{all}}}. \quad (22)$$

With a slight abuse of notations, we define S_{all} as the volume of total parameter space of (x_U, y_U, ϕ) , and S_{coll} as the volume of parameters space of (x_U, y_U, ϕ) which permit an intersection between a 2D spherocylinder and a grid. Rewriting S_{coll} as Eq.(9), we define $S_{\text{coll}}(x)$, $S_{\text{coll}}(y)$, and $S_{\text{coll}}(x, y)$ here as the volume of the parameter space of (x_U, y_U, ϕ) which lead to an intersection between a 2D spherocylinder and a grid cell on the boundaries of the grid cell along the y -axis, the x -axis, and the x - and y -axes at the same time, respectively. Based on Eqs.(1), (2), and (6), and following the derivation in Eqs.(10)-(12), we have

$$\begin{aligned} S_{\text{coll}}(x) &= \int_0^{\frac{\pi}{2}} d\phi \left[\int_0^{\frac{\sigma}{2}} dx + \int_{\frac{\sigma}{2}}^{a-\frac{\sigma}{2}} \Theta \left(l \cos \phi - x + \frac{\sigma}{2} \right) dx + \int_{a-\frac{\sigma}{2}}^a dx \right] \int_0^b dy \\ &+ \int_{\frac{\pi}{2}}^{\pi} d\phi \left[\int_0^{\frac{\sigma}{2}} dx + \int_{\frac{\sigma}{2}}^{a-\frac{\sigma}{2}} \Theta \left(-l \cos \phi + x + \frac{\sigma}{2} - a \right) dx + \int_{a-\frac{\sigma}{2}}^a dx \right] \int_0^b dy \\ &= b \int_0^{\pi} d\phi \int_0^{a-\sigma} \Theta(|l \cos \phi| - x) dx + \sigma b \pi. \end{aligned} \quad (23)$$

$$\begin{aligned} S_{\text{coll}}(y) &= \int_0^{\pi} d\phi \int_0^a dx \left[\int_0^{\frac{\sigma}{2}} dy + \int_{\frac{\sigma}{2}}^{b-\frac{\sigma}{2}} \Theta \left(l \sin \phi - y + \frac{\sigma}{2} \right) dy + \int_{b-\frac{\sigma}{2}}^b dy \right] \\ &= a \int_0^{\pi} d\phi \int_0^{b-\sigma} \Theta(l \sin \phi - y) dy + \sigma a \pi, \end{aligned} \quad (24)$$

$$\begin{aligned} S_{\text{coll}}(x, y) &= \int_0^{\frac{\pi}{2}} d\phi \left[\int_0^{\frac{\sigma}{2}} dx + \int_{\frac{\sigma}{2}}^{a-\frac{\sigma}{2}} \Theta \left(l \cos \phi - x + \frac{\sigma}{2} \right) dx + \int_{a-\frac{\sigma}{2}}^a dx \right] \\ &\times \left[\int_0^{\frac{\sigma}{2}} dy + \int_{\frac{\sigma}{2}}^{b-\frac{\sigma}{2}} \Theta \left(l \sin \phi - y + \frac{\sigma}{2} \right) dy + \int_{b-\frac{\sigma}{2}}^b dy \right] \\ &+ \int_{\frac{\pi}{2}}^{\pi} d\phi \left[\int_0^{\frac{\sigma}{2}} dx + \int_{\frac{\sigma}{2}}^{a-\frac{\sigma}{2}} \Theta \left(-l \cos \phi + x + \frac{\sigma}{2} - a \right) dx + \int_{a-\frac{\sigma}{2}}^a dx \right] \\ &\times \left[\int_0^{\frac{\sigma}{2}} dy + \int_{\frac{\sigma}{2}}^{b-\frac{\sigma}{2}} \Theta \left(l \sin \phi - y + \frac{\sigma}{2} \right) dy + \int_{b-\frac{\sigma}{2}}^b dy \right] \\ &= \int_0^{\pi} d\phi \int_0^{a-\sigma} \Theta(|l \cos \phi| - x) dx \int_0^{b-\sigma} \Theta(l \sin \phi - y) dy \\ &+ \sigma \int_0^{\pi} d\phi \int_0^{a-\sigma} \Theta(|l \cos \phi| - x) dx + \sigma \int_0^{\pi} d\phi \int_0^{b-\sigma} \Theta(l \sin \phi - y) dy + \sigma^2 \pi. \end{aligned} \quad (25)$$

In the above equations, we expand the brackets and further make some rearrangement in integrals with a change of variables. With $x - \frac{\sigma}{2} \rightarrow \hat{x}$, we have

$$\int_{\frac{\sigma}{2}}^{a-\frac{\sigma}{2}} \Theta \left(l \cos \phi - x + \frac{\sigma}{2} \right) dx = \int_0^{a-\sigma} \Theta (l \cos \phi - \hat{x}) d\hat{x}. \quad (26)$$

With $x + \frac{\sigma}{2} - a \rightarrow -\hat{x}$, we have

$$\begin{aligned} \int_{\frac{\sigma}{2}}^{a-\frac{\sigma}{2}} \Theta \left(-l \cos \phi + x + \frac{\sigma}{2} - a \right) dx &= \int_{a-\sigma}^0 \Theta (-l \cos \phi - \hat{x}) d(-\hat{x}) \\ &= \int_0^{a-\sigma} \Theta (-l \cos \phi - \hat{x}) d\hat{x}. \end{aligned} \quad (27)$$

With $y - \frac{\sigma}{2} \rightarrow \hat{y}$, we have

$$\int_{\frac{\sigma}{2}}^{b-\frac{\sigma}{2}} \Theta \left(l \sin \phi - y + \frac{\sigma}{2} \right) dy = \int_0^{b-\sigma} \Theta (l \sin \phi - \hat{y}) d\hat{y}. \quad (28)$$

With the definitions in Eqs. (16)-(18), we reformulate Eqs. (23)-(25) as

$$S_{\text{coll}}(x) = bA(l, a - \sigma) + \sigma b\pi, \quad (29)$$

$$S_{\text{coll}}(y) = aB(l, b - \sigma) + \sigma a\pi, \quad (30)$$

$$S_{\text{coll}}(x, y) = AB(l, a - \sigma, b - \sigma) + \sigma A(l, a - \sigma) + \sigma B(l, b - \sigma) + \sigma^2\pi. \quad (31)$$

Correspondingly, we have

$$S_{\text{coll}} = (b - \sigma)A(l, a - \sigma) + (a - \sigma)B(l, b - \sigma) - AB(l, a - \sigma, b - \sigma) + (\sigma a + \sigma b - \sigma^2)\pi. \quad (32)$$

With the explicit forms of Eqs.(16)-(18) in Appendix A, we can directly derive the result of Eq.(32), and finally $P(l, \sigma, a, b)$. We leave details of calculation in Appendix C. With Eqs.(C.4), (C.6), (C.8), and (C.10), we lay down our final equations as

$$P(l, \sigma, a, b) = \begin{cases} \frac{2}{\pi} \frac{b-\sigma}{b} \frac{l}{a} + \frac{2}{\pi} \frac{a-\sigma}{a} \frac{l}{b} - \frac{1}{\pi} \frac{l^2}{ab} + \left(\frac{\sigma}{a} + \frac{\sigma}{b} - \frac{\sigma^2}{ab} \right), & \text{if } l \leq b - \sigma; \\ \frac{1}{\pi} \frac{(b-\sigma)^2}{ab} + \frac{2}{\pi} \frac{a-\sigma}{a} \frac{l}{b} \left[1 - \sqrt{1 - \frac{(b-\sigma)^2}{l^2}} \right] \\ + \frac{2}{\pi} \frac{a-\sigma}{a} \frac{b-\sigma}{b} \left(\frac{\pi}{2} - \arcsin \frac{b-\sigma}{l} \right) + \left(\frac{\sigma}{a} + \frac{\sigma}{b} - \frac{\sigma^2}{ab} \right), & \text{if } b - \sigma < l \leq a - \sigma; \\ \frac{1}{\pi} \left(\frac{\hat{L}^2}{ab} + \frac{l^2}{ab} \right) - \frac{2}{\pi} \left[\frac{b-\sigma}{b} \frac{l}{a} \sqrt{1 - \frac{(a-\sigma)^2}{l^2}} + \frac{a-\sigma}{a} \frac{l}{b} \sqrt{1 - \frac{(b-\sigma)^2}{l^2}} \right] \\ + \frac{2}{\pi} \frac{a-\sigma}{a} \frac{b-\sigma}{b} \left(\pi - \arcsin \frac{a-\sigma}{l} - \arcsin \frac{b-\sigma}{l} \right) + \left(\frac{\sigma}{a} + \frac{\sigma}{b} - \frac{\sigma^2}{ab} \right), & \text{if } a - \sigma < l \leq \hat{L}; \\ 1, & \text{if } \hat{L} < l, \end{cases} \quad (33)$$

in which we define $\hat{L} \equiv \sqrt{(a - \sigma)^2 + (b - \sigma)^2}$.

We find that when $l > \hat{L}$, $P(l, \sigma, a, b) = 1$. This result has a similar intuitive interpretation with the case of $l > L$ in the 2D needle version. When a 2D spherocylinder can be fitted in a grid cell, its largest length corresponds to the situation when it aligns with the diagonal line of the grid cell and its two semicircles touch the grid boundaries at two opposite corners. This length of a spherocylinder is simply \hat{L} . Thus any 2D spherocylinder with a length $l > \hat{L}$ dropped on a grid is certain to intersect with grid lines, leading to $P(l, \sigma, a, b) = 1$.

We then check the consistency of Eq.(33) for $P(l, \sigma, a, b)$, and equivalently S_{coll} , at the boundaries of the four cases of l . We leave the details of calculation in Appendix D.

When $a \rightarrow \infty$, Eq.(33) simplifies to the result for the BNP of 2D spherocylinders as

$$P(l, \sigma, \infty, b) = \begin{cases} \frac{2}{\pi} \frac{l}{b} + \frac{\sigma}{b}, & \text{if } l \leq b - \sigma; \\ \frac{2}{\pi} \frac{l}{b} \left[1 - \sqrt{1 - \frac{(b-\sigma)^2}{l^2}} \right] + \frac{2}{\pi} \frac{b-\sigma}{b} \left(\frac{\pi}{2} - \arcsin \frac{b-\sigma}{l} \right) + \frac{\sigma}{b}, & \text{if } b - \sigma < l. \end{cases} \quad (34)$$

V. THEORY OF BLNP WITH 3D NEEDLES

We follow the analytical framework for the BLNP with 2D needles. We define $S_{\text{all}}^{3\text{D}}$ as the volume of total parameter space of $(x_{\text{U}}, y_{\text{U}}, \psi, \phi)$ in the case of 3D needles, and $S_{\text{coll}}^{3\text{D}}$ as the volume of proper parameter space of $(x_{\text{U}}, y_{\text{U}}, \psi, \phi)$ where an intersection happens. The intersection probability is thus

$$P^{3\text{D}}(l, a, b) = \frac{S_{\text{coll}}^{3\text{D}}}{S_{\text{all}}^{3\text{D}}}. \quad (35)$$

For $S_{\text{all}}^{3\text{D}}$, we easily have

$$S_{\text{all}}^{3\text{D}} = ab\pi\frac{\pi}{2}. \quad (36)$$

$S_{\text{coll}}^{3\text{D}}$ can be reformulated as

$$S_{\text{coll}}^{3\text{D}} = S_{\text{coll}}^{3\text{D}}(x) + S_{\text{coll}}^{3\text{D}}(y) - S_{\text{coll}}^{3\text{D}}(x, y), \quad (37)$$

while $S_{\text{coll}}^{3\text{D}}(x)$, $S_{\text{coll}}^{3\text{D}}(y)$, and $S_{\text{coll}}^{3\text{D}}(x, y)$ denote the volume of the parameter space of $(x_{\text{U}}, y_{\text{U}}, \psi, \phi)$ when an intersection between the projection of a 3D needle and a grid cell happens on the boundaries of the grid cell along the y -axis, the x -axis, and the x - and y -axes at the same time, respectively. Based on Eqs.(3)-(5), we substitute l with $l \sin \psi$ and put an extra $\int_0^{\pi/2} d\psi$ on each term in Eqs.(10)-(12). We have

$$S_{\text{coll}}^{3\text{D}}(x) = b \int_0^{\pi/2} d\psi \int_0^{\pi} d\phi \int_0^a \Theta(|l \sin \psi \cos \phi| - x) dx, \quad (38)$$

$$S_{\text{coll}}^{3\text{D}}(y) = a \int_0^{\pi/2} d\psi \int_0^{\pi} d\phi \int_0^b \Theta(l \sin \psi \sin \phi - y) dy, \quad (39)$$

$$S_{\text{coll}}^{3\text{D}}(x, y) = \int_0^{\pi/2} d\psi \int_0^{\pi} d\phi \int_0^a \Theta(|l \sin \psi \cos \phi| - x) dx \int_0^b \Theta(l \sin \psi \sin \phi - y) dy. \quad (40)$$

To compute the above equations, we define integrals like Eqs.(16)-(18) as

$$A^{3\text{D}}(l, a) \equiv \int_0^{\pi/2} d\psi \int_0^{\pi} d\phi \int_0^a \Theta(|l \sin \psi \cos \phi| - x) dx, \quad (41)$$

$$B^{3\text{D}}(l, b) \equiv \int_0^{\pi/2} d\psi \int_0^{\pi} d\phi \int_0^b \Theta(l \sin \psi \sin \phi - y) dy, \quad (42)$$

$$AB^{3\text{D}}(l, a, b) \equiv \int_0^{\pi/2} d\psi \int_0^{\pi} d\phi \int_0^a \Theta(|l \sin \psi \cos \phi| - x) dx \int_0^b \Theta(l \sin \psi \sin \phi - y) dy. \quad (43)$$

Thus we reformulate $S_{\text{coll}}^{3\text{D}}$ as

$$S_{\text{coll}}^{3\text{D}} = bA^{3\text{D}}(l, a) + aB^{3\text{D}}(l, b) - AB^{3\text{D}}(l, a, b). \quad (44)$$

To calculate above equations, a thorough analysis of the relative size among l , a , and b should be carried out, in which ψ is considered in different regions in integration. We leave details of calculation in Appendix E. With

Eqs.(E.16), (E.23), (E.31), and (E.36), we lay down our final equations as

$$P^{3D}(l, a, b) = \begin{cases} \left[\frac{4}{\pi^2} \left(\frac{l}{a} + \frac{l}{b} \right) - \frac{1}{2\pi} \frac{l^2}{ab}, \right. & \text{if } l \leq b; \\ \left. \frac{4}{\pi^2} \frac{l}{a} + \left[\frac{4}{\pi^2} \frac{l}{b} - \frac{4}{\pi^2} \frac{l}{b} F\left(\arcsin \frac{b}{l}, \frac{\pi}{2}, \frac{b}{l}\right) + \frac{4}{\pi^2} G\left(\arcsin \frac{b}{l}, \frac{\pi}{2}, \frac{b}{l}\right) \right] \right. & \text{if } b < l \leq a; \\ \left. \frac{4}{\pi^2} \frac{l}{a} - \frac{4}{\pi^2} \frac{l}{a} F\left(\arcsin \frac{a}{l}, \frac{\pi}{2}, \frac{a}{l}\right) + \frac{4}{\pi^2} G\left(\arcsin \frac{a}{l}, \frac{\pi}{2}, \frac{a}{l}\right) \right] & \\ + \left[\frac{4}{\pi^2} \frac{l}{b} - \frac{4}{\pi^2} \frac{l}{b} F\left(\arcsin \frac{b}{l}, \frac{\pi}{2}, \frac{b}{l}\right) + \frac{4}{\pi^2} G\left(\arcsin \frac{b}{l}, \frac{\pi}{2}, \frac{b}{l}\right) \right] & \\ - \left[\frac{1}{\pi^2} \frac{l^2}{ab} \arcsin \frac{a}{l} + \frac{3}{\pi^2} \frac{l}{b} \sqrt{1 - \frac{a^2}{l^2}} - \frac{2}{\pi^2} \frac{a}{b} \left(\frac{\pi}{2} - \arcsin \frac{a}{l} \right) \right] & \\ - \left[\frac{1}{\pi^2} \frac{l^2}{ab} \arcsin \frac{b}{l} + \frac{3}{\pi^2} \frac{l}{a} \sqrt{1 - \frac{b^2}{l^2}} - \frac{2}{\pi^2} \frac{b}{a} \left(\frac{\pi}{2} - \arcsin \frac{b}{l} \right) \right] & + \frac{1}{2\pi} \frac{l^2}{ab}, & \text{if } a < l \leq L; \quad (45) \\ \left. \frac{4}{\pi^2} \frac{l}{a} - \frac{4}{\pi^2} \frac{l}{a} F\left(\arcsin \frac{a}{l}, \arcsin \frac{L}{l}, \frac{a}{l}\right) + \frac{4}{\pi^2} G\left(\arcsin \frac{a}{l}, \arcsin \frac{L}{l}, \frac{a}{l}\right) \right] & \\ + \left[\frac{4}{\pi^2} \frac{l}{b} - \frac{4}{\pi^2} \frac{l}{b} F\left(\arcsin \frac{b}{l}, \arcsin \frac{L}{l}, \frac{b}{l}\right) + \frac{4}{\pi^2} G\left(\arcsin \frac{b}{l}, \arcsin \frac{L}{l}, \frac{b}{l}\right) \right] & \\ - \left[\frac{1}{\pi^2} \frac{l^2}{ab} \arcsin \frac{a}{l} + \frac{3}{\pi^2} \frac{l}{b} \sqrt{1 - \frac{a^2}{l^2}} - \frac{2}{\pi^2} \frac{a}{b} \left(\frac{\pi}{2} - \arcsin \frac{a}{l} \right) \right] & \\ - \left[\frac{1}{\pi^2} \frac{l^2}{ab} \arcsin \frac{b}{l} + \frac{3}{\pi^2} \frac{l}{a} \sqrt{1 - \frac{b^2}{l^2}} - \frac{2}{\pi^2} \frac{b}{a} \left(\frac{\pi}{2} - \arcsin \frac{b}{l} \right) \right] & \\ + \left[\frac{1}{\pi^2} \frac{l^2}{ab} \arcsin \frac{L}{l} - \frac{1}{\pi^2} \frac{lL}{ab} \sqrt{1 - \frac{L^2}{l^2}} - \frac{2}{\pi^2} \frac{L^2}{ab} \left(\frac{\pi}{2} - \arcsin \frac{L}{l} \right) \right] & + \frac{2}{\pi} \left(\frac{\pi}{2} - \arcsin \frac{L}{l} \right), & \text{if } L < l, \end{cases}$$

in which two integrals $F(a, b, t)$ and $G(a, b, t)$ are defined as Eqs.(E.5) and (E.6), respectively.

We can check the consistency of Eq.(45) for $P^{3D}(l, a, b)$, and equivalently S_{coll}^{3D} , at the boundaries of the four cases of l . We leave details of calculation in Appendix F.

We then consider the case of $l \rightarrow \infty$. Calculation in Appendix G shows that, only when $l \rightarrow \infty$, we have $P^{3D}(\infty, a, b) = 1$. This is intuitively understandable. The projection of a finite long needle onto a 2D plane eludes the boundaries of a grid cell with a non-vanishing probability, since the orientation ψ always has a finite, even narrow, range to trigger an intersection. Only an infinitely long needle is sure to intersect with the grid.

When $a \rightarrow \infty$, Eq.(45) simplifies to the result for the BNP with 3D needles as

$$P^{3D}(l, \infty, b) = \begin{cases} \frac{4}{\pi^2} \frac{l}{b}, & \text{if } l \leq b; \\ \frac{4}{\pi^2} \frac{l}{b} - \frac{4}{\pi^2} \frac{l}{b} F\left(\arcsin \frac{b}{l}, \frac{\pi}{2}, \frac{b}{l}\right) + \frac{4}{\pi^2} G\left(\arcsin \frac{b}{l}, \frac{\pi}{2}, \frac{b}{l}\right), & \text{if } b < l. \end{cases} \quad (46)$$

VI. THEORY OF BLNP WITH 3D SPHEROCYLINDERS

We follow the framework for the BLNP with 3D needles, and calculate the intersection probability for the BLNP with 3D spherocylinders here as

$$P^{3D}(l, \sigma, a, b) = \frac{S_{\text{coll}}^{3D}}{S_{\text{all}}^{3D}}. \quad (47)$$

S_{coll}^{3D} can be further reformulated as Eq.(37). $S_{\text{coll}}^{3D}(x)$, $S_{\text{coll}}^{3D}(y)$, and $S_{\text{coll}}^{3D}(x, y)$ denote the volume of the parameter space of (x_U, y_U, ψ, ϕ) when an intersection between the projection of a 3D spherocylinder and a grid cell happens on the boundaries of the grid cell along the y -axis, the x -axis, and the x - and y -axes at the same time, respectively. Based on Eqs. (3), (4), and (6), we move from l to $l \sin \psi$ and add an extra $\int_0^{\pi/2} d\psi$ to each term of Eqs.(23)-(25). We have

$$S_{\text{coll}}^{3D}(x) = b \int_0^{\frac{\pi}{2}} d\psi \int_0^{\pi} d\phi \int_0^{a-\sigma} \Theta(|l \sin \psi \cos \phi| - x) dx + \sigma b \frac{\pi^2}{2}. \quad (48)$$

$$S_{\text{coll}}^{3D}(y) = a \int_0^{\frac{\pi}{2}} d\psi \int_0^{\pi} d\phi \int_0^{b-\sigma} \Theta(l \sin \psi \sin \phi - y) dy + \sigma a \frac{\pi^2}{2}, \quad (49)$$

$$\begin{aligned} S_{\text{coll}}^{3D}(x, y) &= \int_0^{\frac{\pi}{2}} d\psi \int_0^{\pi} d\phi \int_0^{a-\sigma} \Theta(|l \sin \psi \cos \phi| - x) dx \int_0^{b-\sigma} \Theta(l \sin \psi \sin \phi - y) dy \\ &+ \sigma \int_0^{\frac{\pi}{2}} d\psi \int_0^{\pi} d\phi \int_0^{a-\sigma} \Theta(|l \sin \psi \cos \phi| - x) dx + \sigma \int_0^{\frac{\pi}{2}} d\psi \int_0^{\pi} d\phi \int_0^{b-\sigma} \Theta(l \sin \psi \sin \phi - y) dy \\ &+ \sigma^2 \frac{\pi^2}{2}. \end{aligned} \quad (50)$$

With the definitions in Eqs.(41)-(43), we have

$$S_{\text{coll}}^{3\text{D}}(x) = bA^{3\text{D}}(l, a - \sigma) + \sigma b \frac{\pi^2}{2}, \quad (51)$$

$$S_{\text{coll}}^{3\text{D}}(y) = aB^{3\text{D}}(l, b - \sigma) + \sigma a \frac{\pi^2}{2}, \quad (52)$$

$$S_{\text{coll}}^{3\text{D}}(x, y) = AB^{3\text{D}}(l, a - \sigma, b - \sigma) + \sigma A^{3\text{D}}(l, a - \sigma) + \sigma B^{3\text{D}}(l, b - \sigma) + \sigma^2 \frac{\pi^2}{2}. \quad (53)$$

Equivalently, we have

$$S_{\text{coll}}^{3\text{D}} = (b - \sigma)A^{3\text{D}}(l, a - \sigma) + (a - \sigma)B^{3\text{D}}(l, b - \sigma) - AB^{3\text{D}}(l, a - \sigma, b - \sigma) + (\sigma a + \sigma b - \sigma^2) \frac{\pi^2}{2}. \quad (54)$$

With the explicit forms of $A^{3\text{D}}(l, a)$, $B^{3\text{D}}(l, b)$ and $AB^{3\text{D}}(l, a, b)$ in Appendix E, we can easily lay down $S_{\text{coll}}^{3\text{D}}$ with Eq.(54), and finally $P^{3\text{D}}(l, \sigma, a, b)$. We leave details of calculation in Appendix H. With Eqs.(H.5), (H.7), (H.9), and (H.11), we list our final equations as

$$P^{3\text{D}}(l, \sigma, a, b) = \begin{cases} \left[\frac{4}{\pi^2} \frac{b-\sigma}{b} \frac{l}{a} + \frac{4}{\pi^2} \frac{a-\sigma}{a} \frac{l}{b} - \frac{1}{2\pi} \frac{l^2}{ab} + \left(\frac{\sigma}{a} + \frac{\sigma}{b} - \frac{\sigma^2}{ab} \right), \right. & \text{if } l \leq b - \sigma; \\ \left[\frac{4}{\pi^2} \frac{b-\sigma}{b} \frac{l}{a} + \left[\frac{4}{\pi^2} \frac{a-\sigma}{a} \frac{l}{b} - \frac{4}{\pi^2} \frac{a-\sigma}{a} \frac{l}{b} F \left(\arcsin \frac{b-\sigma}{l}, \frac{\pi}{2}, \frac{b-\sigma}{l} \right) + \frac{4}{\pi^2} \frac{a-\sigma}{a} \frac{b-\sigma}{b} G \left(\arcsin \frac{b-\sigma}{l}, \frac{\pi}{2}, \frac{b-\sigma}{l} \right) \right] \right. \\ \left. - \left[\frac{1}{\pi^2} \frac{l^2}{ab} \arcsin \frac{b-\sigma}{l} + \frac{3}{\pi^2} \frac{b-\sigma}{b} \frac{l}{a} \sqrt{1 - \frac{(b-\sigma)^2}{l^2}} - \frac{2}{\pi^2} \frac{(b-\sigma)^2}{ab} \left(\frac{\pi}{2} - \arcsin \frac{b-\sigma}{l} \right) \right] + \left(\frac{\sigma}{a} + \frac{\sigma}{b} - \frac{\sigma^2}{ab} \right), \right. & \text{if } b - \sigma < l \leq a - \sigma; \\ \left[\frac{4}{\pi^2} \frac{b-\sigma}{b} \frac{l}{a} - \frac{4}{\pi^2} \frac{b-\sigma}{b} \frac{l}{a} F \left(\arcsin \frac{a-\sigma}{l}, \frac{\pi}{2}, \frac{a-\sigma}{l} \right) + \frac{4}{\pi^2} \frac{a-\sigma}{a} \frac{b-\sigma}{b} G \left(\arcsin \frac{a-\sigma}{l}, \frac{\pi}{2}, \frac{a-\sigma}{l} \right) \right] \\ + \left[\frac{4}{\pi^2} \frac{a-\sigma}{a} \frac{l}{b} - \frac{4}{\pi^2} \frac{a-\sigma}{a} \frac{l}{b} F \left(\arcsin \frac{b-\sigma}{l}, \frac{\pi}{2}, \frac{b-\sigma}{l} \right) + \frac{4}{\pi^2} \frac{a-\sigma}{a} \frac{b-\sigma}{b} G \left(\arcsin \frac{b-\sigma}{l}, \frac{\pi}{2}, \frac{b-\sigma}{l} \right) \right] \\ - \left[\frac{1}{\pi^2} \frac{l^2}{ab} \arcsin \frac{a-\sigma}{l} + \frac{3}{\pi^2} \frac{a-\sigma}{a} \frac{l}{b} \sqrt{1 - \frac{(a-\sigma)^2}{l^2}} - \frac{2}{\pi^2} \frac{(a-\sigma)^2}{ab} \left(\frac{\pi}{2} - \arcsin \frac{a-\sigma}{l} \right) \right] \\ - \left[\frac{1}{\pi^2} \frac{l^2}{ab} \arcsin \frac{b-\sigma}{l} + \frac{3}{\pi^2} \frac{b-\sigma}{b} \frac{l}{a} \sqrt{1 - \frac{(b-\sigma)^2}{l^2}} - \frac{2}{\pi^2} \frac{(b-\sigma)^2}{ab} \left(\frac{\pi}{2} - \arcsin \frac{b-\sigma}{l} \right) \right] \\ + \frac{1}{2\pi} \frac{l^2}{ab} + \left(\frac{\sigma}{a} + \frac{\sigma}{b} - \frac{\sigma^2}{ab} \right), & \text{if } a - \sigma < l \leq \hat{L}; \\ \left[\frac{4}{\pi^2} \frac{b-\sigma}{b} \frac{l}{a} - \frac{4}{\pi^2} \frac{b-\sigma}{b} \frac{l}{a} F \left(\arcsin \frac{a-\sigma}{l}, \arcsin \frac{\hat{L}}{l}, \frac{a-\sigma}{l} \right) + \frac{4}{\pi^2} \frac{a-\sigma}{a} \frac{b-\sigma}{b} G \left(\arcsin \frac{a-\sigma}{l}, \arcsin \frac{\hat{L}}{l}, \frac{a-\sigma}{l} \right) \right] \\ + \left[\frac{4}{\pi^2} \frac{a-\sigma}{a} \frac{l}{b} - \frac{4}{\pi^2} \frac{a-\sigma}{a} \frac{l}{b} F \left(\arcsin \frac{b-\sigma}{l}, \arcsin \frac{\hat{L}}{l}, \frac{b-\sigma}{l} \right) + \frac{4}{\pi^2} \frac{a-\sigma}{a} \frac{b-\sigma}{b} G \left(\arcsin \frac{b-\sigma}{l}, \arcsin \frac{\hat{L}}{l}, \frac{b-\sigma}{l} \right) \right] \\ - \left[\frac{1}{\pi^2} \frac{l^2}{ab} \arcsin \frac{a-\sigma}{l} + \frac{3}{\pi^2} \frac{a-\sigma}{a} \frac{l}{b} \sqrt{1 - \frac{(a-\sigma)^2}{l^2}} - \frac{2}{\pi^2} \frac{(a-\sigma)^2}{ab} \left(\frac{\pi}{2} - \arcsin \frac{a-\sigma}{l} \right) \right] \\ - \left[\frac{1}{\pi^2} \frac{l^2}{ab} \arcsin \frac{b-\sigma}{l} + \frac{3}{\pi^2} \frac{b-\sigma}{b} \frac{l}{a} \sqrt{1 - \frac{(b-\sigma)^2}{l^2}} - \frac{2}{\pi^2} \frac{(b-\sigma)^2}{ab} \left(\frac{\pi}{2} - \arcsin \frac{b-\sigma}{l} \right) \right] \\ + \left[\frac{1}{\pi^2} \frac{l^2}{ab} \arcsin \frac{\hat{L}}{l} - \frac{1}{\pi^2} \frac{l\hat{L}}{ab} \sqrt{1 - \frac{\hat{L}^2}{l^2}} - \frac{2}{\pi^2} \frac{\hat{L}^2}{ab} \left(\frac{\pi}{2} - \arcsin \frac{\hat{L}}{l} \right) \right] \\ + \frac{2}{\pi} \frac{a-\sigma}{a} \frac{b-\sigma}{b} \left(\frac{\pi}{2} - \arcsin \frac{\hat{L}}{l} \right) + \left(\frac{\sigma}{a} + \frac{\sigma}{b} - \frac{\sigma^2}{ab} \right), & \text{if } \hat{L} < l. \end{cases} \quad (55)$$

We further check the consistency of Eq.(55) for $P^{3\text{D}}(l, \sigma, a, b)$, and equivalently $S_{\text{coll}}^{3\text{D}}$, on the boundaries of four cases of l . We leave details of calculation in Appendix I.

We then consider the limit case of $l \rightarrow \infty$. In Appendix J, we show that, just like the case of infinitely long 3D needles, only a 3D spherocylinder with an infinitely large length l intersect with a grid with a probability of 1.

When $a \rightarrow \infty$, Eq. (55) simplifies to the result for the BNP of 3D spherocylinders as

$$P^{3\text{D}}(l, \sigma, \infty, b) = \begin{cases} \frac{4}{\pi^2} \frac{l}{b} + \frac{\sigma}{b}, & \text{if } l \leq b - \sigma; \\ \frac{4}{\pi^2} \frac{l}{b} - \frac{4}{\pi^2} \frac{l}{b} F \left(\arcsin \frac{b-\sigma}{l}, \frac{\pi}{2}, \frac{b-\sigma}{l} \right) + \frac{4}{\pi^2} \frac{b-\sigma}{b} G \left(\arcsin \frac{b-\sigma}{l}, \frac{\pi}{2}, \frac{b-\sigma}{l} \right) + \frac{\sigma}{b}, & \text{if } b - \sigma < l. \end{cases} \quad (56)$$

VII. COMPARISON WITH PREVIOUS RESULTS

First, our Eq.(20) with $l \leq b$ retrieves the result for the ‘short’ needle case of $l < b$ for BLNP with 2D needles in [9, 10, 17].

Then, we can see that Eq.(21), which corresponds to the case of $a \rightarrow \infty$ in our theory for BLNP with 2D needles, corresponds to the result for the original BNP with arbitrary length l in [17].

We further compare our results on BLNP with those in [8] with a special case of $a = b = 1$. Eq.(6) in [8] shows the intersection probability in BLNP with 2D needles under $b < l$. Based on Eq.(20) in the case of $a < l \leq L$ and setting $a = b = 1$, we have

$$P(l, 1, 1) = 1 - \frac{2}{\pi} \left(\arcsin \frac{1}{l} - \arccos \frac{1}{l} + 2\sqrt{l^2 - 1} - \frac{l^2}{2} - 1 \right). \quad (57)$$

We can easily find that there is an error in Eq.(6) in [8] as the coefficient $1/\pi$ of the second term should be $2/\pi$ as we show above.

Besides, Eq.(8) in [8] presents the intersection probability in BLNP with 2D spherocylinders in the case of small l . With Eq.(33) in the case of $l \leq b - \sigma$ and setting $a = b = 1$, we have

$$P(l, \sigma, 1, 1) = \frac{4l - l^2}{\pi} + \frac{\sigma}{\pi}(-4l + 2\pi - \sigma\pi). \quad (58)$$

The difference between Eq.(8) in [8] and our above prediction is

$$\Delta P = \frac{\sigma}{\pi}(-4 + 3\sigma + 2l). \quad (59)$$

It is easy to see that, when $\sigma \ll 1$, we have $\Delta P < 0$. Yet when $\sigma \approx l \approx 1$, we have instead $\Delta P > 0$. As all our analytical results can be validated in the following section, we believe that there is probably an error in the derivation of Eq.(8) in [8].

VIII. RESULT

Our final analytical equations are summed in Eqs.(20), (21), (33), (34), (45), (46), (55), and (56). There are two points we should mention. The first one is that, the intersection probabilities depend only on the relative sizes of dropped objects and grids, say l , σ , a , and b , not their sizes per se. The second one is that, to calculate an intersection probability there are four regimes separated by three length scales, each with a specific analytical form. To verify the correctness of our analytical predictions, we perform Monte Carlo simulation of dropping objects for given finite l , σ , a , and b explained in Section II, and compare these empirical intersection probability with theoretical predictions from our analytical framework.

To numerically calculate integrals, there is a large toolbox in existing literature we can refer to. Here for simplicity we adopt the classical Simpson's rule [31] for Eqs. (E.5) and (E.6). We can see that the integrands in both integrals have a closed form. We divide the range $[a, b]$ into equally spaced intervals with a size $[(b-a) \times N_{\text{unit}} \times 2i]$ with $i = 1, 2, \dots$, and calculate a sequence of numerical summations $F(i)$ based on Simpson's rule. When $|F(i+1) - F(i)| < \varepsilon$, we consider $F(i+1)$ as our numerical approximation of an integral. In this section, we set $N_{\text{unit}} = 10^4$ and $\varepsilon = 10^{-9}$.

We first consider how the sizes of needles and spherocylinders affect an intersection probability. Fig.2 shows both results from numerical simulation and analytical theory. As we can see, an intersection probability increases monotonously with a larger length for a needle or a larger length and radius for a spherocylinder once the other size parameters are fixed. Besides, a comparison between Fig.2 (a)-(c) with (d)-(f) shows that, the introduction of a new degree of freedom for a dropped object generally pushes down intersection probability. The profile of intersection probability further changes drastically in the case of long objects: in the 2D cases, objects with a length beyond a finite critical value is sure to intersect with grid lines, while in the 3D cases only infinitely long objects intersect with grid lines with probability 1.

We should also mention that, for our equations of intersection probabilities, a naive extrapolation of an analytical form in a certain region to a different one with a larger l only leads to an overestimation of intersection probability, until there is an unphysical result as the probability goes beyond 1.

From a different perspective, we further consider how an intersection probability evolves with the aspect ratio of grid cell a/b . This context is highly relevant when we consider irregular filter in a filtration process. With our theory, we can locate those parameters leading to the maximal flux (correspondingly the minimal intersection probability), which can be further tested in a controlled experiment. We define a dimensionless control parameter $\lambda \equiv l^2/ab$, and calculate intersection probability with tuned λ . Given the control coefficient λ , the radius ratio σ/l ($\equiv \sigma_l$), and the aspect ratio a/b ($\equiv t$), a correspondence between parameters can be established as

$$\left(\frac{l}{a}, \frac{l}{b}, \frac{\sigma}{a}, \frac{\sigma}{b} \right) = \left(\sqrt{\frac{\lambda}{t}}, \sqrt{\lambda t}, \sigma_l \sqrt{\frac{\lambda}{t}}, \sigma_l \sqrt{\lambda t} \right). \quad (60)$$

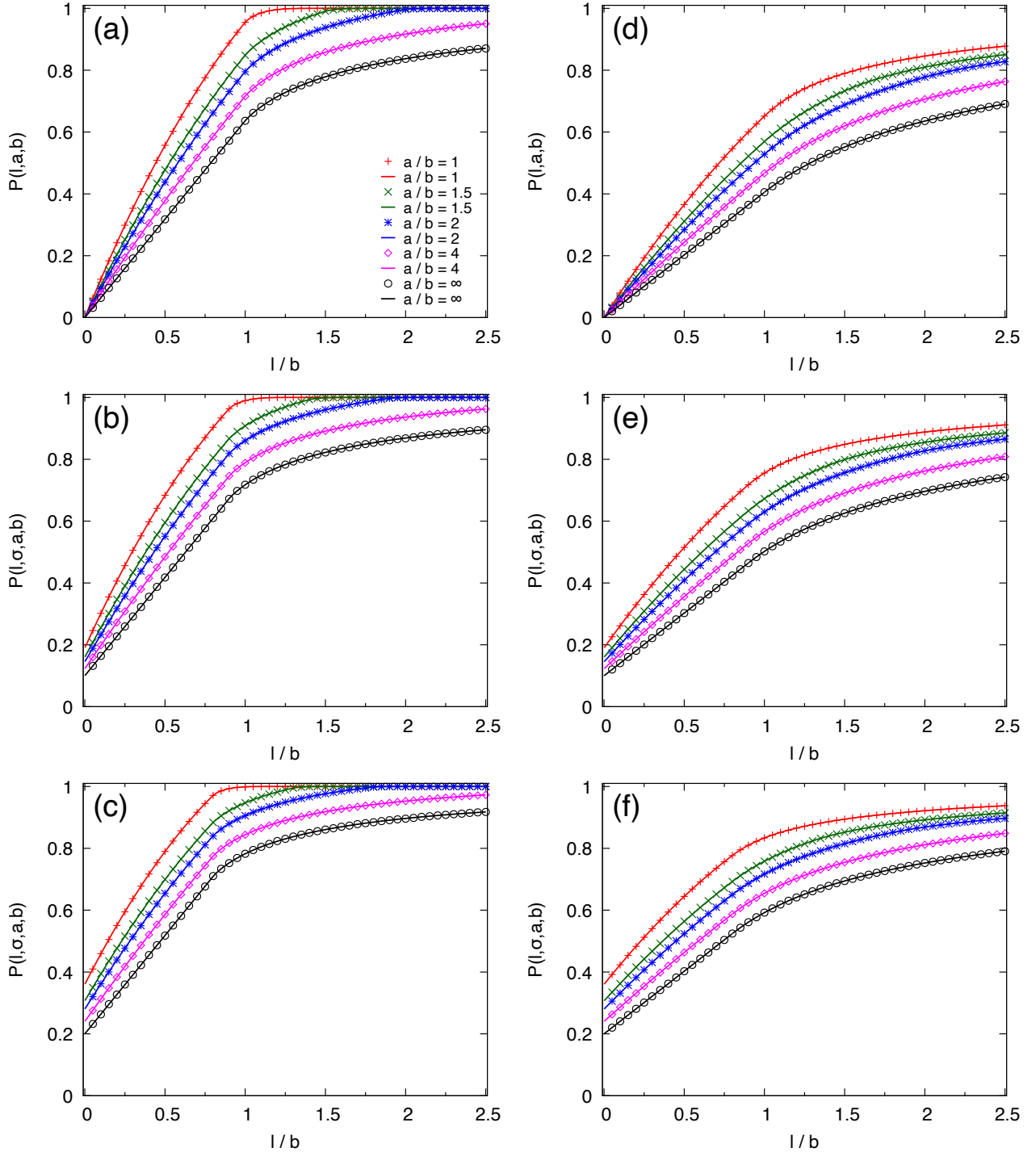


FIG. 2. Result of BLNP with needles and spherocylinders with fixed height b of a grid cell. (a) The intersection probability $P(l, a, b)$ versus the ratio l/b is shown in the case of 2D needles. (b)-(c) The intersection probability $P(l, \sigma, a, b)$ versus l/b is shown in the case of 2D spherocylinders with $\sigma/b = 0.1$ and 0.2 , respectively. (d)-(f) Results are shown in the same format as (a)-(c), yet for the case of 3D needles and spherocylinders. In each subfigure, we show results when $a/b = 1, 1.5, 2, 4, \infty$, the last of which simply corresponds to the BNP version. Each sign is from result of a single Monte Carlo simulation with $b = 3$ and a configuration size $N_{\text{all}} = 10^6$ for the 2D case and $N_{\text{all}} = 10^7$ for the 3D case. Solid lines are from analytical results.

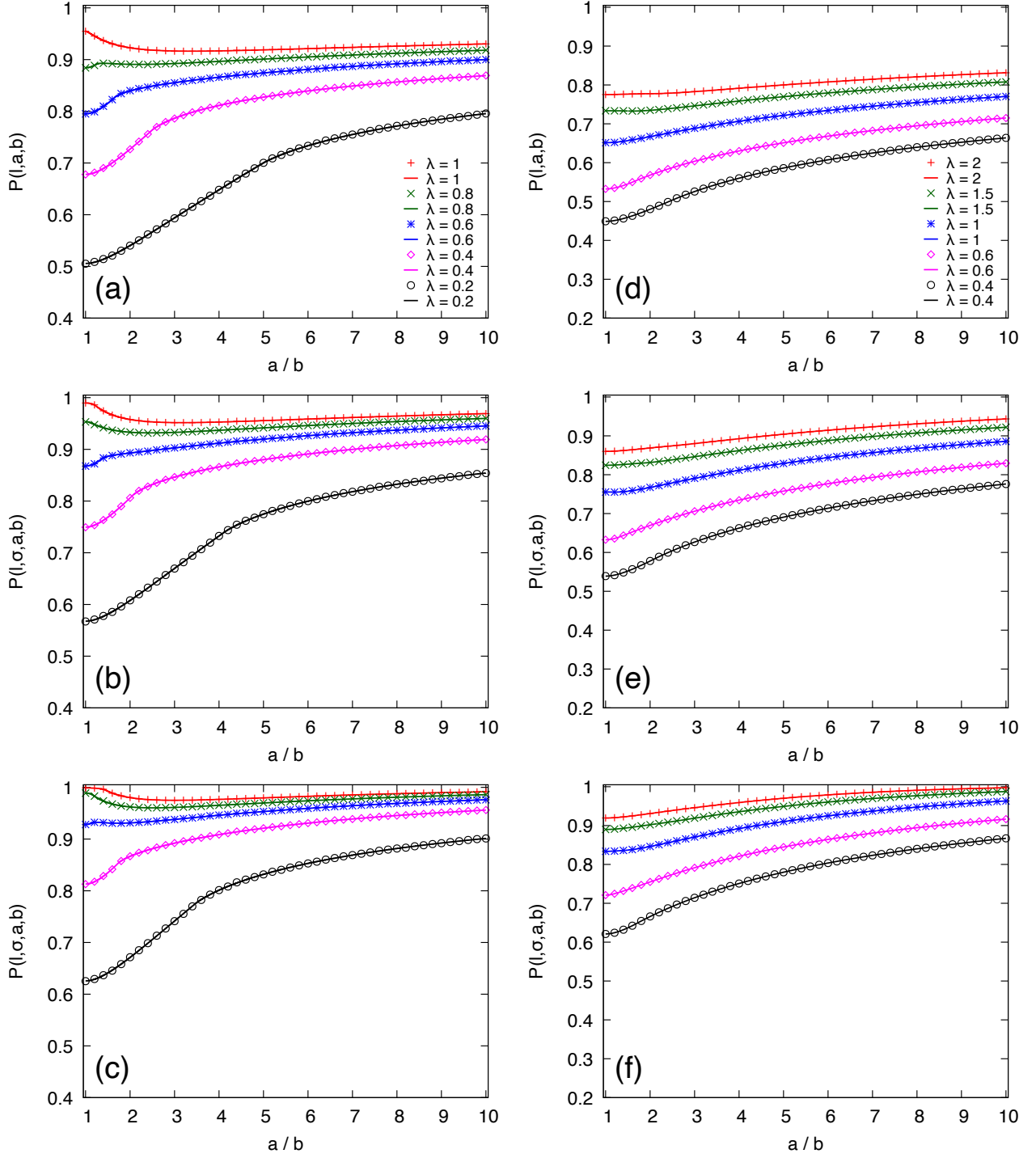


FIG. 3. Result of BLNP with needles and spherocylinders with fixed area ab of a grid cell. (a) The intersection probability $P(l, a, b)$ versus the ratio a/b is shown in the case of 2D needles. (b)-(c) The intersection probability $P(l, \sigma, a, b)$ versus a/b is shown in the case of 2D spherocylinders with $\sigma/l = 0.1$ and 0.2 , respectively. In each subfigure of (a)-(c), we show results when $\lambda = 1, 0.8, 0.6, 0.4, 0.2$. (d)-(f) Results are shown in the same format as (a)-(c), yet for the cases of 3D needles and spherocylinders. In each subfigure of (d)-(f), we show results when $\lambda = 2, 1.5, 1, 0.6, 0.4$. Each sign is from result of a single Monte Carlo simulation with $l = 3$ and a configuration size $N_{\text{all}} = 10^6$ for the 2D case and $N_{\text{all}} = 10^7$ for the 3D case. Solid lines are from analytical results.

Fig.3 shows both simulation and analytical result. Unlike the pattern of monotonously increasing intersection probability in Fig.2, we can find a much more complicated picture.

Results in Fig.3 (a)-(c) for 2D cases follow a quite similar pattern, as we can find a local minimum moving from $t = 1$ to some $t > 1$ with increasing λ . We present a possible qualitative scenario here: (1) when $\lambda \leq \lambda_1^*$, there is only one local minimum of intersection probability, which is exactly at $t_1 = 1$; (2) when $\lambda_1^* < \lambda \leq \lambda_2^*$, a second local minimum emerges at $t_2 > 1$, and a hump-like shape with a local maximum separates the two minima, yet the global minimum still happens at $t_1 = 1$; (3) when $\lambda_2^* < \lambda \leq \lambda_3^*$, the two local minima still coexists as in (2), yet the global minimum moves from $t_1 = 1$ to $t_2 > 1$; (4) when $\lambda_3^* < \lambda$, the local minimum at $t_1 = 1$ vanishes, and the local minimum at $t_2 > 1$ becomes the global one. For Fig.3 (a), we test λ numerically and find that $\lambda_1^* \approx 0.771$, $\lambda_2^* \approx 0.830$, and $\lambda_3^* \approx 0.999$. An intuitive understanding of the scenario is that, with an increasing a/b and a grid cell becoming more elongated, there is a competition between a decrease in the intersection probability due to a larger width a and an increase in the intersection probability due to a smaller height b of the grid cell. Yet the dominant term in the competition simply depends on the control parameter λ . The above scenario of moving minimum is much like the one in the analysis of critical transitions and hysteresis with a stability landscape in a multiple stable system (see Fig.(2.6) in [32]), while the two minima here correspond to the two stable equilibrium states of the system and the control parameter λ acts as the strength of an external perturbation on the system.

Results in Fig.3 (d)-(f) for 3D cases follow a much more smooth way than those in the 2D cases. In most cases in Fig.3 (d)-(f), $t = 1$ is the global minimum for intersection probability. Yet we can still numerically find a different global minimum at $t > 1$. For example, in Fig.3 (d) for the case of 3D needles with $\lambda = 1.5$, we have $P(l, a, b) = 0.733559$ at $t = 1$ and a smaller $P(l, a, b) = 0.732816$ at $t = 1.605$.

For Fig.3, there still remains some fundamental questions to resolve, such as to theoretically ascertain the scenario of moving minimum in 2D cases, to analytically locate the global minimum with any given λ in the 2D cases, and to prove whether the results in the 3D cases still follow the scenario in the 2D cases. To fully resolve these questions, we need to carry out a detailed analysis of landscapes of intersection probabilities with respect to t . Due to the current amount of theoretical analysis and results in this paper, we would like to leave them to a future work.

IX. CONCLUSION

Here we analytically study BLNP in different versions on their intersection probabilities. With a single probabilistic framework, we solve problem versions with dropped objects, with increasing analytical complexity, from a 2D needle with arbitrary length l to a 3D spherocylinder with arbitrary length l and diameter σ onto a grid with any width a and height b . Our analytical predictions are further validated by Monte Carlo simulation.

For the filtration process, our analytical results here only describe the contact probability between particles and a mesh upon the arrival of particles in flow. To fully construct a probabilistic picture of a filtration process [5], a number of considerations should be combined into current models. First, multiple contacts between a particle with a mesh with the center of mass between contacts leads to a caught particle on a mesh, and an analytical theory for the distribution of number of intersections is highly relevant for an analysis of caking [7]. Then, after a contact with a mesh, a particle slightly rotates due to a torque from the mesh and finally leads to a collective effect with other particles to induce clogging [8]. Additional terms can be incorporated into our model to account the dynamical effect from the interaction between particles and a mesh. Although highly mathematically involved, the above considerations represent essential steps towards a full analytical picture of filtration process. We leave the related treatment in future works.

Besides, there are already many extensions of BLNP with physical backgrounds. Our analytical framework here, which applies to any shape size of needles and spherocylinders, helps to pave the way for principled theoretical approaches into untested parameter regions for these generalizations and variants.

ACKNOWLEDGEMENTS

This work is supported by Guangdong Basic and Applied Basic Research Foundation (Grant No. 2022A1515011765), Guangdong Major Project of Basic and Applied Basic Research No. 2020B0301030008, and National Natural Science Foundation of China (Grant No. 12171479).

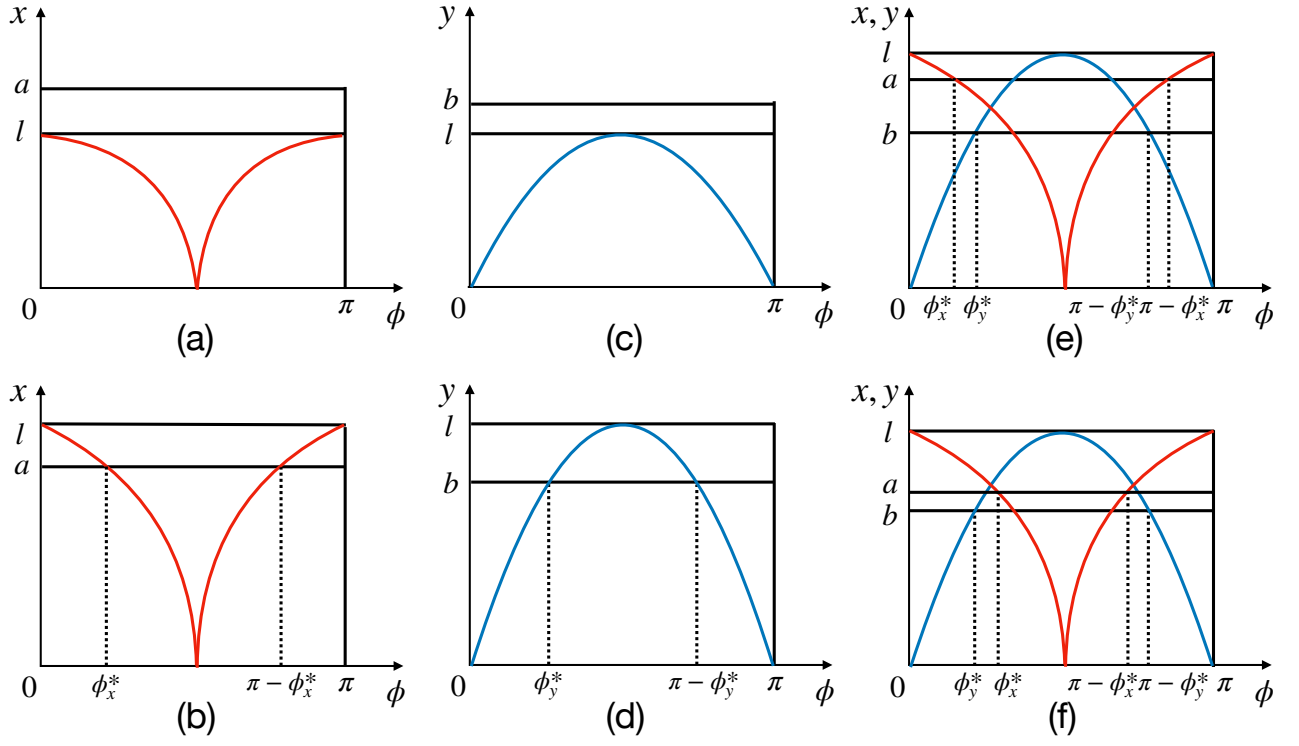


FIG. 4. Relative sizes among l , a , and b for $A(l, a)$, $B(l, b)$, and $AB(l, a, b)$. (a)-(b) The curve $x = |l \cos \phi|$ is shown under the conditions of $l \leq a$ and $a < l$, respectively. $\phi_x^* \in (0, \pi/2)$ and $\pi - \phi_x^*$ are the ϕ -coordinates at which the lines $x = |l \cos \phi|$ and $x = a$ overlap. (c)-(d) The curve $y = l \sin \phi$ is shown under the conditions of $l \leq b$ and $b < l$, respectively. $\phi_y^* \in (0, \pi/2)$ and $\pi - \phi_y^*$ are the ϕ -coordinates at which the lines $y = l \sin \phi$ and $y = b$ overlap. (e)-(f) The curves $x = |l \cos \phi|$ and $y = l \sin \phi$ are shown at the same time under the conditions of $\phi_x^* \leq \phi_y^*$, equivalently $l \leq L$, and $\phi_y^* < \phi_x^*$, equivalently $L < l$, respectively.

X. APPENDIX A: CALCULATION FOR THEORY OF BLNP WITH 2D NEEDLES

We can find that the integrals in Eqs.(16)-(18) has a simple form as

$$\int_0^t \Theta(m - z) dz = \min\{t, m\}, \quad (\text{A.1})$$

in which $(t, m, z) = (a, |l \cos \phi|, x)$ and $(b, l \sin \phi, y)$.

We write $A(l, a)$ in the case of $l \leq a$ and $a < l$ respectively as $A(l, a|l \leq a)$ and $A(l, a|a < l)$. When $l \leq a$, $|l \cos \phi| \leq a$ always holds for $\phi \in [0, \pi]$. Yet when $a < l$, $|l \cos \phi| \leq a$ holds only when $\phi \in [\phi_x^*, \pi - \phi_x^*]$, in which we define

$$\phi_x^* = \arccos \frac{a}{l}. \quad (\text{A.2})$$

See Fig.4 (a) and (b) for an illustration. We have

$$\begin{aligned} A(l, a|l \leq a) &= \int_0^{\frac{\pi}{2}} d\phi \cdot l \cos \phi + \int_{\frac{\pi}{2}}^{\pi} d\phi \cdot (-l \cos \phi) \\ &= 2l, \end{aligned} \quad (\text{A.3})$$

$$\begin{aligned} A(l, a|a < l) &= \int_0^{\phi_x^*} d\phi \cdot a + \int_{\phi_x^*}^{\frac{\pi}{2}} d\phi \cdot l \cos \phi + \int_{\frac{\pi}{2}}^{\pi - \phi_x^*} d\phi \cdot (-l \cos \phi) + \int_{\pi - \phi_x^*}^{\pi} d\phi \cdot a \\ &= 2l(1 - \sin \phi_x^*) + 2a\phi_x^*. \end{aligned} \quad (\text{A.4})$$

We then write $B(l, b)$ in the case of $l \leq b$ and $b < l$ respectively as $B(l, b|l \leq b)$ and $B(l, b|b < l)$. When $l \leq b$, $l \sin \phi \leq b$ always holds for $\phi \in [0, \pi]$. Yet when $b < l$, $l \sin \phi \leq b$ holds only when $\phi \in [0, \phi_y^*] \cup [\pi - \phi_y^*, \pi]$, in which

we define

$$\phi_y^* = \arcsin \frac{b}{l}. \quad (\text{A.5})$$

See Fig.4 (c) and (d) for an illustration. We have

$$\begin{aligned} B(l, b|l \leq b) &= \int_0^\pi d\phi \cdot l \sin \phi \\ &= 2l, \end{aligned} \quad (\text{A.6})$$

$$\begin{aligned} B(l, b|b < l) &= \int_0^{\phi_y^*} d\phi \cdot l \sin \phi + \int_{\phi_y^*}^{\pi - \phi_y^*} d\phi \cdot b + \int_{\pi - \phi_y^*}^\pi d\phi \cdot l \sin \phi \\ &= 2l (1 - \cos \phi_y^*) + 2b \left(\frac{\pi}{2} - \phi_y^* \right). \end{aligned} \quad (\text{A.7})$$

To calculate $AB(l, a, b)$ and finally $P(l, a, b)$, the relative sizes among (l, a, b) are more involved. We will detail four cases below.

A. The case of $l \leq b$

We write $AB(l, a, b)$ when $l \leq b$ as $AB(l, a, b|l \leq b)$. With Eq.(18) we have

$$\begin{aligned} AB(l, a, b|l \leq b) &= \int_0^{\frac{\pi}{2}} d\phi \cdot l \cos \phi \cdot l \sin \phi + \int_{\frac{\pi}{2}}^\pi d\phi \cdot (-l \cos \phi) \cdot l \sin \phi \\ &= l^2. \end{aligned} \quad (\text{A.8})$$

With Eq.(19) we then have

$$\begin{aligned} S_{\text{coll}} &= bA(l, a|l \leq a) + aB(l, b|l \leq b) - AB(l, a, b|l \leq b) \\ &= 2lb + 2la - l^2. \end{aligned} \quad (\text{A.9})$$

We thus have

$$P(l, a, b) = \frac{2}{\pi} \left(\frac{l}{a} + \frac{l}{b} \right) - \frac{1}{\pi} \frac{l^2}{ab}. \quad (\text{A.10})$$

B. The case of $b < l \leq a$

We write $AB(l, a, b)$ when $b < l \leq a$ as $AB(l, a, b|b < l \leq a)$. We have

$$\begin{aligned} AB(l, a, b|b < l \leq a) &= \int_0^{\phi_y^*} d\phi \cdot l \cos \phi \cdot l \sin \phi + \int_{\phi_y^*}^{\frac{\pi}{2}} d\phi \cdot l \cos \phi \cdot b \\ &\quad + \int_{\frac{\pi}{2}}^{\pi - \phi_y^*} d\phi \cdot (-l \cos \phi) \cdot b + \int_{\pi - \phi_y^*}^\pi d\phi \cdot (-l \cos \phi) \cdot l \sin \phi \\ &= 2lb - b^2. \end{aligned} \quad (\text{A.11})$$

Then,

$$\begin{aligned} S_{\text{coll}} &= bA(l, a|l \leq a) + aB(l, b|b < l) - AB(l, a, b|b < l \leq a) \\ &= b^2 + 2la(1 - \cos \phi_y^*) + 2ab \left(\frac{\pi}{2} - \phi_y^* \right) \\ &= b^2 + 2la \left(1 - \sqrt{1 - \frac{b^2}{l^2}} \right) + 2ab \left(\frac{\pi}{2} - \arcsin \frac{b}{l} \right). \end{aligned} \quad (\text{A.12})$$

We thus have

$$P(l, a, b) = \frac{1}{\pi} \frac{b}{a} + \frac{2}{\pi} \frac{l}{b} \left(1 - \sqrt{1 - \frac{b^2}{l^2}} \right) + \frac{2}{\pi} \left(\frac{\pi}{2} - \arcsin \frac{b}{l} \right). \quad (\text{A.13})$$

C. The cases in $a < l$

To further calculate $AB(l, a, b)$, we should check the relative size between ϕ_x^* and ϕ_y^* . When $a < l \leq L$, we have $1 - a^2/l^2 \leq b^2/l^2$. Equivalently we have $\sin^2 \phi_x^* \leq \sin^2 \phi_y^*$, correspondingly $\phi_x^* \leq \phi_y^*$. See Fig.4 (e) for an illustration. Here we write $AB(l, a, b)$ when $a < l \leq L$ as $AB(l, a, b|a < l \leq L)$. We have

$$\begin{aligned}
AB(l, a, b|a < l \leq L) &= \int_0^{\phi_x^*} d\phi \cdot a \cdot l \sin \phi + \int_{\phi_x^*}^{\phi_y^*} d\phi \cdot l \cos \phi \cdot l \sin \phi + \int_{\phi_y^*}^{\frac{\pi}{2}} d\phi \cdot l \cos \phi \cdot b \\
&+ \int_{\frac{\pi}{2}}^{\pi - \phi_y^*} d\phi \cdot (-l \cos \phi) \cdot b + \int_{\pi - \phi_y^*}^{\pi - \phi_x^*} d\phi \cdot (-l \cos \phi) \cdot l \sin \phi + \int_{\pi - \phi_x^*}^{\pi} d\phi \cdot a \cdot l \sin \phi \\
&= 2la + 2lb - L^2 - l^2.
\end{aligned} \tag{A.14}$$

Then,

$$\begin{aligned}
S_{\text{coll}} &= bA(l, a|a < l) + aB(l, b|b < l) - AB(l, a, b|a < l \leq L) \\
&= L^2 + l^2 - 2lb \sin \phi_x^* - 2la \cos \phi_y^* + 2ab \left(\phi_x^* + \frac{\pi}{2} - \phi_y^* \right) \\
&= L^2 + l^2 - 2 \left(lb \sqrt{1 - \frac{a^2}{l^2}} + la \sqrt{1 - \frac{b^2}{l^2}} \right) + 2ab \left(\pi - \arcsin \frac{a}{l} - \arcsin \frac{b}{l} \right).
\end{aligned} \tag{A.15}$$

Correspondingly,

$$P(l, a, b) = \frac{1}{\pi} \left(\frac{L^2}{ab} + \frac{l^2}{ab} \right) - \frac{2}{\pi} \left(\frac{l}{a} \sqrt{1 - \frac{a^2}{l^2}} + \frac{l}{b} \sqrt{1 - \frac{b^2}{l^2}} \right) + \frac{2}{\pi} \left(\pi - \arcsin \frac{a}{l} - \arcsin \frac{b}{l} \right). \tag{A.16}$$

When $L < l$, we have $\phi_y^* < \phi_x^*$ equivalently. We write $AB(l, a, b)$ when $L < l$ as $AB(l, a, b|L < l)$. We have

$$\begin{aligned}
AB(l, a, b|L < l) &= \int_0^{\phi_y^*} d\phi \cdot a \cdot l \sin \phi + \int_{\phi_y^*}^{\phi_x^*} d\phi \cdot a \cdot b + \int_{\phi_x^*}^{\frac{\pi}{2}} d\phi \cdot l \cos \phi \cdot b \\
&+ \int_{\frac{\pi}{2}}^{\pi - \phi_x^*} d\phi \cdot (-l \cos \phi) \cdot b + \int_{\pi - \phi_x^*}^{\pi - \phi_y^*} d\phi \cdot a \cdot b + \int_{\pi - \phi_y^*}^{\pi} d\phi \cdot a \cdot l \sin \phi \\
&= 2la(1 - \cos \phi_y^*) + 2lb(1 - \sin \phi_x^*) + 2ab(\phi_x^* - \phi_y^*).
\end{aligned} \tag{A.17}$$

Then,

$$\begin{aligned}
S_{\text{coll}} &= bA(l, a|a < l) + aB(l, b|b < l) - AB(l, a, b|L < l) \\
&= ab\pi,
\end{aligned} \tag{A.18}$$

after most terms cancel out. Correspondingly, we have

$$P(l, a, b) = 1. \tag{A.19}$$

XI. APPENDIX B: CONSISTENCY OF EQUATIONS IN THEORY OF BLNP WITH 2D NEEDLES

When $l = 0$, in the case of $l \leq b$, we have

$$S_{\text{coll}} = 0, \tag{B.1}$$

which is quite intuitive.

When $l = b$, both S_{coll} in the cases of $l \leq b$ and $b < l \leq a$ reduce to

$$S_{\text{coll}} = b^2 + 2ab. \tag{B.2}$$

When $l = a$, both S_{coll} in the cases of $b < l \leq a$ and $a < l \leq L$ reduce to

$$S_{\text{coll}} = b^2 + 2a^2 \left(1 - \sqrt{1 - \frac{b^2}{a^2}} \right) + 2ab \left(\frac{\pi}{2} - \arcsin \frac{b}{a} \right). \quad (\text{B.3})$$

When $l = L$, S_{coll} in the case of $a < l \leq L$ reduces to

$$S_{\text{coll}} = ab\pi, \quad (\text{B.4})$$

which equals S_{coll} in the case of $L < l$ in Eq.(A.18).

XII. APPENDIX C: CALCULATION FOR THEORY OF BLNP WITH 2D SPHEROCYLINDERS

As Eqs.(A.2) and (A.5), we first define here

$$\hat{\phi}_x^* = \arccos \frac{a - \sigma}{l}, \quad (\text{C.1})$$

$$\hat{\phi}_y^* = \arcsin \frac{b - \sigma}{l}. \quad (\text{C.2})$$

When $l \leq b - \sigma$, we have

$$\begin{aligned} S_{\text{coll}} &= (b - \sigma)A(l, a - \sigma | l \leq a - \sigma) + (a - \sigma)B(l, b - \sigma | l \leq b - \sigma) \\ &\quad - AB(l, a - \sigma, b - \sigma | l \leq b - \sigma) + (\sigma a + \sigma b - \sigma^2) \pi \\ &= 2l(b - \sigma) + 2l(a - \sigma) - l^2 + (\sigma a + \sigma b - \sigma^2) \pi. \end{aligned} \quad (\text{C.3})$$

Thus,

$$P(l, \sigma, a, b) = \frac{2}{\pi} \frac{b - \sigma}{b} \frac{l}{a} + \frac{2}{\pi} \frac{a - \sigma}{a} \frac{l}{b} - \frac{1}{\pi} \frac{l^2}{ab} + \left(\frac{\sigma}{a} + \frac{\sigma}{b} - \frac{\sigma^2}{ab} \right). \quad (\text{C.4})$$

When $b - \sigma < l \leq a - \sigma$, we have

$$\begin{aligned} S_{\text{coll}} &= (b - \sigma)A(l, a - \sigma | l \leq a - \sigma) + (a - \sigma)B(l, b - \sigma | b - \sigma < l) \\ &\quad - AB(l, a - \sigma, b - \sigma | b - \sigma < l \leq a - \sigma) + (\sigma a + \sigma b - \sigma^2) \pi \\ &= (b - \sigma)^2 + 2l(a - \sigma)(1 - \cos \hat{\phi}_y^*) + 2(a - \sigma)(b - \sigma) \left(\frac{\pi}{2} - \hat{\phi}_y^* \right) + (\sigma a + \sigma b - \sigma^2) \pi \\ &= (b - \sigma)^2 + 2l(a - \sigma) \left[1 - \sqrt{1 - \frac{(b - \sigma)^2}{l^2}} \right] + 2(a - \sigma)(b - \sigma) \left(\frac{\pi}{2} - \arcsin \frac{b - \sigma}{l} \right) + (\sigma a + \sigma b - \sigma^2) \pi. \end{aligned} \quad (\text{C.5})$$

Thus,

$$\begin{aligned} P(l, \sigma, a, b) &= \frac{1}{\pi} \frac{(b - \sigma)^2}{ab} + \frac{2}{\pi} \frac{a - \sigma}{a} \frac{l}{b} \left[1 - \sqrt{1 - \frac{(b - \sigma)^2}{l^2}} \right] \\ &\quad + \frac{2}{\pi} \frac{a - \sigma}{a} \frac{b - \sigma}{b} \left(\frac{\pi}{2} - \arcsin \frac{b - \sigma}{l} \right) + \left(\frac{\sigma}{a} + \frac{\sigma}{b} - \frac{\sigma^2}{ab} \right). \end{aligned} \quad (\text{C.6})$$

When $a - \sigma < l \leq \hat{L}$, we have $\hat{\phi}_x^* \leq \hat{\phi}_y^*$ correspondingly. Then

$$\begin{aligned} S_{\text{coll}} &= (b - \sigma)A(l, a - \sigma | a - \sigma < l) + (a - \sigma)B(l, b - \sigma | b - \sigma < l) \\ &\quad - AB(l, a - \sigma, b - \sigma | a - \sigma < l \leq \hat{L}) + (\sigma a + \sigma b - \sigma^2) \pi \\ &= \hat{L}^2 + l^2 - 2l(b - \sigma) \sin \hat{\phi}_x^* - 2l(a - \sigma) \cos \hat{\phi}_y^* \\ &\quad + 2(a - \sigma)(b - \sigma) \left(\hat{\phi}_x^* + \frac{\pi}{2} - \hat{\phi}_y^* \right) + (\sigma a + \sigma b - \sigma^2) \pi \\ &= \hat{L}^2 + l^2 - 2l(b - \sigma) \sqrt{1 - \frac{(a - \sigma)^2}{l^2}} - 2l(a - \sigma) \sqrt{1 - \frac{(b - \sigma)^2}{l^2}} \\ &\quad + 2(a - \sigma)(b - \sigma) \left(\pi - \arcsin \frac{a - \sigma}{l} - \arcsin \frac{b - \sigma}{l} \right) + (\sigma a + \sigma b - \sigma^2) \pi. \end{aligned} \quad (\text{C.7})$$

Thus,

$$\begin{aligned}
P(l, \sigma, a, b) &= \frac{1}{\pi} \left(\frac{\hat{L}^2}{ab} + \frac{l^2}{ab} \right) - \frac{2}{\pi} \left[\frac{b-\sigma}{b} \frac{l}{a} \sqrt{1 - \frac{(a-\sigma)^2}{l^2}} + \frac{a-\sigma}{a} \frac{l}{b} \sqrt{1 - \frac{(b-\sigma)^2}{l^2}} \right] \\
&\quad + \frac{2}{\pi} \frac{a-\sigma}{a} \frac{b-\sigma}{b} \left(\pi - \arcsin \frac{a-\sigma}{l} - \arcsin \frac{b-\sigma}{l} \right) + \left(\frac{\sigma}{a} + \frac{\sigma}{b} - \frac{\sigma^2}{ab} \right). \tag{C.8}
\end{aligned}$$

When $\hat{L} < l$, we have $\hat{\phi}_y^* < \hat{\phi}_x^*$. Then,

$$\begin{aligned}
S_{\text{coll}} &= (b-\sigma)A(l, a-\sigma|a-\sigma < l) + (a-\sigma)B(l, b-\sigma|b-\sigma < l) \\
&\quad - AB(l, a-\sigma, b-\sigma|\hat{L} < l) + (\sigma a + \sigma b - \sigma^2) \pi \\
&= ab\pi. \tag{C.9}
\end{aligned}$$

Thus,

$$P(l, \sigma, a, b) = 1. \tag{C.10}$$

XIII. APPENDIX D: CONSISTENCY OF EQUATIONS IN THEORY OF BLNP WITH 2D SPHEROCYLINDERS

When $l = 0$, in the case of $l \leq b - \sigma$ we have

$$S_{\text{coll}} = (\sigma a + \sigma b - \sigma^2) \pi. \tag{D.1}$$

Intuitively, a 2D spherocylinder with $l = 0$ reduces to a circle. An intersection between the circle and a grid cell happens when the center of the circle is within a distance of its radius $\sigma/2$ from the four boundaries of the grid cell. We easily have

$$S_{\text{coll}} = [ab - (a-\sigma)(b-\sigma)] \times \pi = (\sigma a + \sigma b - \sigma^2) \pi. \tag{D.2}$$

When $l = b - \sigma$, both S_{coll} in the cases of $l \leq b - \sigma$ and $b - \sigma < l \leq a - \sigma$ reduce to

$$S_{\text{coll}} = (b-\sigma)^2 + 2(a-\sigma)(b-\sigma) + (\sigma a + \sigma b - \sigma^2) \pi. \tag{D.3}$$

When $l = a - \sigma$, both S_{coll} in the cases of $b - \sigma < l \leq a - \sigma$ and $a - \sigma < l \leq \hat{L}$ correspond to

$$\begin{aligned}
S_{\text{coll}} &= (b-\sigma)^2 + 2(a-\sigma)^2 \left[1 - \sqrt{1 - \frac{(b-\sigma)^2}{(a-\sigma)^2}} \right] \\
&\quad + 2(a-\sigma)(b-\sigma) \left(\frac{\pi}{2} - \arcsin \frac{b-\sigma}{a-\sigma} \right) + (\sigma a + \sigma b - \sigma^2) \pi. \tag{D.4}
\end{aligned}$$

When $l = \hat{L}$ in the case of $a - \sigma < l \leq \hat{L}$, we have $\cos^2 \hat{\phi}_x^* + \sin^2 \hat{\phi}_y^* = 1$, equivalently $\hat{\phi}_x^* = \hat{\phi}_y^*$. After some calculation we have

$$S_{\text{coll}} = ab\pi, \tag{D.5}$$

which coincides with the uniform S_{coll} in the case of $\hat{L} < l$ in Eq.(C.9).

XIV. APPENDIX E: CALCULATION FOR THEORY OF BLNP WITH 3D NEEDLES

We first calculate $A(l, a)$ and $B(l, b)$. We write $A^{3D}(l, a)$ when $l \leq a$ and $a < l$ as $A^{3D}(l, a|l \leq a)$ and $A^{3D}(l, a|a < l)$, respectively. When $l \leq a$, $|l \sin \psi \cos \phi| \leq a$ always holds for any $\psi \in [0, \pi/2]$ and $\phi \in [0, \pi]$. We have

$$\begin{aligned}
A^{3D}(l, a|l \leq a) &= \int_0^{\frac{\pi}{2}} d\psi \int_0^{\frac{\pi}{2}} d\phi \cdot l \sin \psi \cos \phi + \int_0^{\frac{\pi}{2}} d\psi \int_{\frac{\pi}{2}}^{\pi} d\phi \cdot (-l \sin \psi \cos \phi) \\
&= 2l, \tag{E.1}
\end{aligned}$$

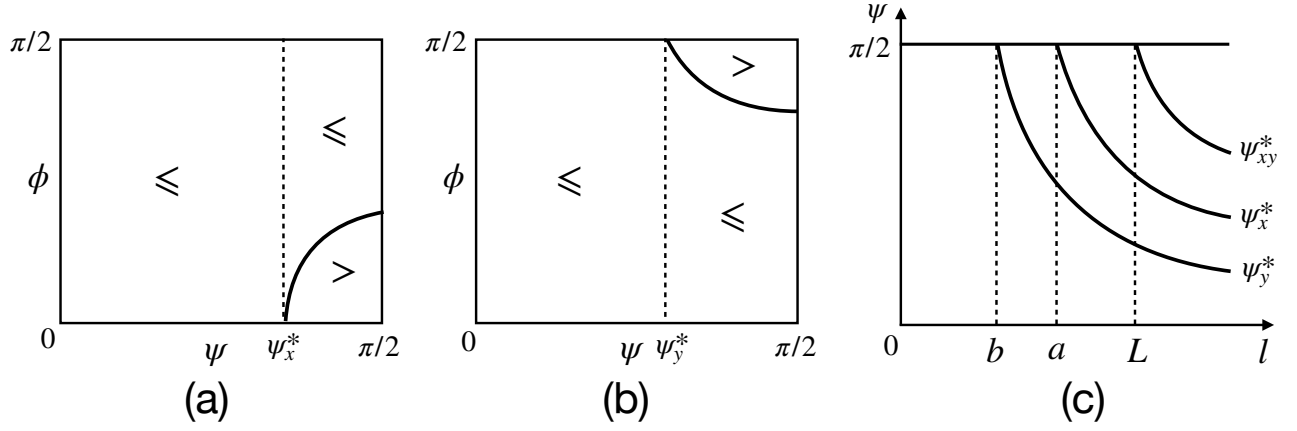


FIG. 5. Schematic diagrams of calculation in the BLNP with 3D needles. (a) The dashed and solid lines correspond to $\psi = \psi_x^*$ and $\phi = \phi_x^*(\psi)$, respectively. The notions \leq and $>$ within diagrams respectively denotes the regions of parameters (ψ, ϕ) in which $l \sin \psi \cos \phi \leq a$ and $l \sin \psi \cos \phi > a$ hold. (b) The dashed and solid lines show $\psi = \psi_y^*$ and $\phi = \phi_y^*(\psi)$, respectively. The notions \leq and $>$ respectively denote the regions of parameters (ψ, ϕ) in which $l \sin \psi \sin \phi \leq b$ and $l \sin \psi \sin \phi > b$ hold. (c) Boundaries of regions ψ_x^* , ψ_y^* , and ψ_{xy}^* , when Eqs.(43) is calculated by integrating on ψ , are shown in the cases of $l \leq b$, $b < l \leq a$, $a < l \leq L$, and $L < l$, respectively.

When $a < l$, the picture is slightly more complicated. We first define

$$\psi_x^* = \arcsin \frac{a}{l}, \quad (\text{E.2})$$

$$\phi_x^*(\psi) = \arccos \frac{a}{l \sin \psi}. \quad (\text{E.3})$$

We can see that, when $\psi \leq \psi_x^*$, we have $l \sin \psi \cos \phi \leq a$ satisfied for any $\phi \in [0, \pi/2]$. Yet when $\psi > \psi_x^*$, two situations happen depending on the value of ϕ : when $\phi \in [\phi_x^*(\psi), \pi/2]$, $l \sin \psi \cos \phi \leq a$ still holds; yet when $\phi \in [0, \phi_x^*(\psi))$, $l \sin \psi \cos \phi > a$ holds instead. A simple schematics is in Fig.5 (a). Later we simply write $\phi_x^*(\psi)$ as ϕ_x^* for short in this section. We have

$$\begin{aligned} A^{3D}(l, a|a < l) &= \int_0^{\psi_x^*} d\psi \int_0^{\frac{\pi}{2}} d\phi \cdot l \sin \psi \cos \phi + \int_0^{\psi_x^*} d\psi \int_{\frac{\pi}{2}}^{\pi} d\phi \cdot (-l \sin \psi \cos \phi) \\ &+ \int_{\psi_x^*}^{\frac{\pi}{2}} d\psi \int_0^{\phi_x^*} d\phi \cdot a + \int_{\psi_x^*}^{\frac{\pi}{2}} d\psi \int_{\phi_x^*}^{\frac{\pi}{2}} d\phi \cdot l \sin \psi \cos \phi \\ &+ \int_{\psi_x^*}^{\frac{\pi}{2}} d\psi \int_{\frac{\pi}{2}}^{\pi - \phi_x^*} d\phi \cdot (-l \sin \psi \cos \phi) + \int_{\psi_x^*}^{\frac{\pi}{2}} d\psi \int_{\pi - \phi_x^*}^{\pi} d\phi \cdot a \\ &= 2l - 2l \int_{\psi_x^*}^{\frac{\pi}{2}} d\psi \sqrt{\sin^2 \psi - \frac{a^2}{l^2}} + 2a \int_{\psi_x^*}^{\frac{\pi}{2}} d\psi \left(\frac{\pi}{2} - \arcsin \frac{a}{l \sin \psi} \right) \\ &= 2l - 2lF\left(\psi_x^*, \frac{\pi}{2}, \frac{a}{l}\right) + 2aG\left(\psi_x^*, \frac{\pi}{2}, \frac{a}{l}\right), \end{aligned} \quad (\text{E.4})$$

in whose last step we define two integrals respectively as

$$F(a, b, t) \equiv \int_a^b d\psi \sqrt{\sin^2 \psi - t^2}, \quad (\text{E.5})$$

$$G(a, b, t) \equiv \int_a^b d\psi \left(\frac{\pi}{2} - \arcsin \frac{t}{\sin \psi} \right). \quad (\text{E.6})$$

These two integrals can be calculated with standard numerical integration methods [31].

We then write $B^{3D}(l, b)$ when $l \leq b$ and $b < l$ as $B^{3D}(l, b|l \leq b)$ and $B^{3D}(l, b|b < l)$, respectively. When $l \leq b$,

$l \sin \psi \sin \phi \leq b$ always hold for any $\psi \in [0, \pi/2]$ and $\phi \in [0, \pi)$. We have

$$\begin{aligned} B^{3D}(l, b|l \leq b) &= \int_0^{\frac{\pi}{2}} d\psi \int_0^{\pi} d\phi \cdot l \sin \psi \sin \phi \\ &= 2l. \end{aligned} \quad (\text{E.7})$$

When $b < l$, as in the case of $a < l$ for $A^{3D}(l, a)$, we first define

$$\psi_y^* = \arcsin \frac{b}{l}, \quad (\text{E.8})$$

$$\phi_y^*(\psi) = \arcsin \frac{b}{l \sin \psi}. \quad (\text{E.9})$$

We can find that, when $\psi \leq \psi_y^*$, $l \sin \psi \sin \phi \leq b$ is satisfied for any $\phi \in [0, \pi/2]$. Yet when $\psi > \psi_y^*$, two situations happen depending on the value of ϕ : when $\phi \in [0, \phi_y^*(\psi)]$, $l \sin \psi \sin \phi \leq b$ still holds; yet when $\phi \in (\phi_y^*(\psi), \pi/2]$, $l \sin \psi \sin \phi > b$ holds instead. A simple schematics is in Fig.5 (b). Later we simply write $\phi_y^*(\psi)$ as ϕ_y^* for short in this section. We have

$$\begin{aligned} B^{3D}(l, b|b < l) &= \int_0^{\psi_y^*} d\psi \int_0^{\pi} d\phi \cdot l \sin \psi \sin \phi \\ &+ \int_{\psi_y^*}^{\frac{\pi}{2}} d\psi \int_0^{\phi_y^*} d\phi \cdot l \sin \psi \sin \phi + \int_{\psi_y^*}^{\frac{\pi}{2}} d\psi \int_{\phi_y^*}^{\pi - \phi_y^*} d\phi \cdot b + \int_{\psi_y^*}^{\frac{\pi}{2}} d\psi \int_{\pi - \phi_y^*}^{\pi} d\phi \cdot l \sin \psi \sin \phi \\ &= 2l - 2l \int_{\psi_y^*}^{\frac{\pi}{2}} d\psi \sqrt{\sin^2 \psi - \frac{b^2}{l^2}} + 2b \int_{\psi_y^*}^{\frac{\pi}{2}} d\psi \left(\frac{\pi}{2} - \arcsin \frac{b}{l \sin \psi} \right) \\ &= 2l - 2lF \left(\psi_y^*, \frac{\pi}{2}, \frac{b}{l} \right) + 2bG \left(\psi_y^*, \frac{\pi}{2}, \frac{b}{l} \right). \end{aligned} \quad (\text{E.10})$$

To further calculate $AB^{3D}(l, a, b)$ and finally $P^{3D}(l, a, b)$, we consider the following four cases.

A. The case of $l \leq b$

Here the range $\psi \in [0, \pi/2]$ represents a simple case in $AB(l, a, b)$, in which $|l \sin \psi \cos \phi| \leq a$ and $l \sin \psi \sin \phi \leq b$ both hold for any $\phi \in [0, \pi)$. See Fig.5(c) for an illustration. We write $AB^{3D}(l, a, b)$ when $l \leq b$ as $AB^{3D}(l, a, b|l \leq b)$. We have

$$\begin{aligned} AB^{3D}(l, a, b|l \leq b) &= \int_0^{\frac{\pi}{2}} d\psi \int_0^{\frac{\pi}{2}} d\phi \cdot l \sin \psi \cos \phi \cdot l \sin \psi \sin \phi + \int_0^{\frac{\pi}{2}} d\psi \int_{\frac{\pi}{2}}^{\pi} d\phi \cdot (-l \sin \psi \cos \phi) \cdot l \sin \psi \sin \phi \\ &= S^{(1)} \left(0, \frac{\pi}{2} \right). \end{aligned} \quad (\text{E.11})$$

In the above equations, we define and calculate a summation as

$$\begin{aligned} S^{(1)}(0, \psi^*) &\equiv \int_0^{\psi^*} d\psi \int_0^{\frac{\pi}{2}} d\phi \cdot l \sin \psi \cos \phi \cdot l \sin \psi \sin \phi + \int_0^{\psi^*} d\psi \int_{\frac{\pi}{2}}^{\pi} d\phi \cdot (-l \sin \psi \cos \phi) \cdot l \sin \psi \sin \phi \\ &= \frac{l^2}{2} (\psi^* - \sin \psi^* \cos \psi^*). \end{aligned} \quad (\text{E.12})$$

Thus we have

$$S^{(1)} \left(0, \frac{\pi}{2} \right) = \frac{\pi}{4} l^2, \quad (\text{E.13})$$

$$S^{(1)}(0, \psi_y^*) = \frac{l^2}{2} \psi_y^* - \frac{lb}{2} \cos \psi_y^*. \quad (\text{E.14})$$

With Eq.(44) we have

$$\begin{aligned} S_{\text{coll}}^{3\text{D}} &= bA^{3\text{D}}(l, a|l \leq a) + aB^{3\text{D}}(l, b|l \leq b) - AB^{3\text{D}}(l, a, b|l \leq b) \\ &= 2lb + 2la - \frac{\pi}{4}l^2. \end{aligned} \quad (\text{E.15})$$

Then,

$$P^{3\text{D}}(l, a, b) = \frac{4}{\pi^2} \left(\frac{l}{a} + \frac{l}{b} \right) - \frac{1}{2\pi} \frac{l^2}{ab}. \quad (\text{E.16})$$

B. The case of $b < l \leq a$

Here we consider the integral on ψ in $AB(l, a, b)$ in two ranges of $[0, \psi_y^*]$ and $(\psi_y^*, \pi/2]$ in a separate way. See Fig.5 (c) for a schematics. We write $AB^{3\text{D}}(l, a, b)$ when $b < l \leq a$ as $AB^{3\text{D}}(l, a, b|b < l \leq a)$. We have

$$\begin{aligned} &AB^{3\text{D}}(l, a, b|b < l \leq a) \\ &= \int_0^{\psi_y^*} d\psi \int_0^{\frac{\pi}{2}} d\phi \cdot l \sin \psi \cos \phi \cdot l \sin \psi \sin \phi + \int_0^{\psi_y^*} d\psi \int_{\frac{\pi}{2}}^{\pi} d\phi \cdot (-l \sin \psi \cos \phi) \cdot l \sin \psi \sin \phi \\ &+ \int_{\psi_y^*}^{\frac{\pi}{2}} d\psi \int_0^{\phi_y^*} d\phi \cdot l \sin \psi \cos \phi \cdot l \sin \psi \sin \phi + \int_{\psi_y^*}^{\frac{\pi}{2}} d\psi \int_{\phi_y^*}^{\frac{\pi}{2}} d\phi \cdot l \sin \psi \cos \phi \cdot b \\ &+ \int_{\psi_y^*}^{\frac{\pi}{2}} d\psi \int_{\frac{\pi}{2}}^{\pi - \phi_y^*} d\phi \cdot (-l \sin \psi \cos \phi) \cdot b + \int_{\psi_y^*}^{\frac{\pi}{2}} d\psi \int_{\pi - \phi_y^*}^{\pi} d\phi \cdot (-l \sin \psi \cos \phi) \cdot l \sin \psi \sin \phi \\ &= S^{(1)}(0, \psi_y^*) + S^{(2)}\left(\psi_y^*, \frac{\pi}{2}\right). \end{aligned} \quad (\text{E.17})$$

In the above equations, we define and calculate a summation as

$$\begin{aligned} S^{(2)}(\psi_y^*, \psi^*) &\equiv \int_{\psi_y^*}^{\psi^*} d\psi \int_0^{\phi_y^*} d\phi \cdot l \sin \psi \cos \phi \cdot l \sin \psi \sin \phi + \int_{\psi_y^*}^{\psi^*} d\psi \int_{\phi_y^*}^{\frac{\pi}{2}} d\phi \cdot l \sin \psi \cos \phi \cdot b \\ &+ \int_{\psi_y^*}^{\psi^*} d\psi \int_{\frac{\pi}{2}}^{\pi - \phi_y^*} d\phi \cdot (-l \sin \psi \cos \phi) \cdot b + \int_{\psi_y^*}^{\psi^*} d\psi \int_{\pi - \phi_y^*}^{\pi} d\phi \cdot (-l \sin \psi \cos \phi) \cdot l \sin \psi \sin \phi \\ &= 2lb(\cos \psi_y^* - \cos \psi^*) - b^2(\psi^* - \psi_y^*). \end{aligned} \quad (\text{E.18})$$

Thus we have

$$S^{(2)}\left(\psi_y^*, \frac{\pi}{2}\right) = 2lb \cos \psi_y^* - b^2 \left(\frac{\pi}{2} - \psi_y^* \right), \quad (\text{E.19})$$

$$S^{(2)}(\psi_y^*, \psi_x^*) = 2lb(\cos \psi_y^* - \cos \psi_x^*) - b^2(\psi_x^* - \psi_y^*). \quad (\text{E.20})$$

Then,

$$AB^{3\text{D}}(l, a, b|b < l \leq a) = \frac{l^2}{2}\psi_y^* + \frac{3}{2}lb \cos \psi_y^* - b^2 \left(\frac{\pi}{2} - \psi_y^* \right). \quad (\text{E.21})$$

We have

$$\begin{aligned} S_{\text{coll}}^{3\text{D}} &= bA^{3\text{D}}(l, a|l \leq a) + aB^{3\text{D}}(l, b|b < l) - AB^{3\text{D}}(l, a, b|b < l \leq a) \\ &= 2lb + \left[2la - 2laF\left(\psi_y^*, \frac{\pi}{2}, \frac{b}{l}\right) + 2abG\left(\psi_y^*, \frac{\pi}{2}, \frac{b}{l}\right) \right] \\ &- \left[\frac{l^2}{2}\psi_y^* + \frac{3}{2}lb \cos \psi_y^* - b^2 \left(\frac{\pi}{2} - \psi_y^* \right) \right] \\ &= 2lb + \left[2la - 2laF\left(\arcsin \frac{b}{l}, \frac{\pi}{2}, \frac{b}{l}\right) + 2abG\left(\arcsin \frac{b}{l}, \frac{\pi}{2}, \frac{b}{l}\right) \right] \\ &- \left[\frac{l^2}{2} \arcsin \frac{b}{l} + \frac{3}{2}lb \sqrt{1 - \frac{b^2}{l^2}} - b^2 \left(\frac{\pi}{2} - \arcsin \frac{b}{l} \right) \right]. \end{aligned} \quad (\text{E.22})$$

Then,

$$\begin{aligned}
P^{3D}(l, a, b) &= \frac{4}{\pi^2} \frac{l}{a} + \left[\frac{4}{\pi^2} \frac{l}{b} - \frac{4}{\pi^2} \frac{l}{b} F\left(\arcsin \frac{b}{l}, \frac{\pi}{2}, \frac{b}{l}\right) + \frac{4}{\pi^2} G\left(\arcsin \frac{b}{l}, \frac{\pi}{2}, \frac{b}{l}\right) \right] \\
&\quad - \left[\frac{1}{\pi^2} \frac{l^2}{ab} \arcsin \frac{b}{l} + \frac{3}{\pi^2} \frac{l}{a} \sqrt{1 - \frac{b^2}{l^2}} - \frac{2}{\pi^2} \frac{b}{a} \left(\frac{\pi}{2} - \arcsin \frac{b}{l}\right) \right].
\end{aligned} \tag{E.23}$$

C. The cases in $a < l$

We consider here two subcases as $a < l \leq L$ and $L < l$. When $a < l \leq L$, we calculate the integral on ψ in $AB(l, a, b)$ in three ranges of $[0, \psi_y^*]$, $(\psi_y^*, \psi_x^*]$, and $(\psi_x^*, \pi/2]$ in a separate way. See Fig.5 (c) for an illustration. We write $AB^{3D}(l, a, b)$ when $a < l \leq L$ as $AB^{3D}(l, a, b|a < l \leq L)$. We have

$$\begin{aligned}
&AB^{3D}(l, a, b|a < l \leq L) \\
&= \int_0^{\psi_y^*} d\psi \int_0^{\frac{\pi}{2}} d\phi \cdot l \sin \psi \cos \phi \cdot l \sin \psi \sin \phi + \int_0^{\psi_y^*} d\psi \int_{\frac{\pi}{2}}^{\pi} d\phi \cdot (-l \sin \psi \cos \phi) \cdot l \sin \psi \sin \phi \\
&+ \int_{\psi_y^*}^{\psi_x^*} d\psi \int_0^{\phi_y^*} d\phi \cdot l \sin \psi \cos \phi \cdot l \sin \psi \sin \phi + \int_{\psi_y^*}^{\psi_x^*} d\psi \int_{\phi_y^*}^{\frac{\pi}{2}} d\phi \cdot l \sin \psi \cos \phi \cdot b \\
&+ \int_{\psi_y^*}^{\psi_x^*} d\psi \int_{\frac{\pi}{2}}^{\pi - \phi_y^*} d\phi \cdot (-l \sin \psi \cos \phi) \cdot b + \int_{\psi_y^*}^{\psi_x^*} d\psi \int_{\pi - \phi_y^*}^{\pi} d\phi \cdot (-l \sin \psi \cos \phi) \cdot l \sin \psi \sin \phi \\
&+ \int_{\psi_x^*}^{\frac{\pi}{2}} d\psi \int_0^{\phi_x^*} d\phi \cdot a \cdot l \sin \psi \sin \phi + \int_{\psi_x^*}^{\frac{\pi}{2}} d\psi \int_{\phi_x^*}^{\phi_y^*} d\phi \cdot l \sin \psi \cos \phi \cdot l \sin \psi \sin \phi \\
&+ \int_{\psi_x^*}^{\frac{\pi}{2}} d\psi \int_{\phi_y^*}^{\frac{\pi}{2}} d\phi \cdot l \sin \psi \cos \phi \cdot b \\
&+ \int_{\psi_x^*}^{\frac{\pi}{2}} d\psi \int_{\frac{\pi}{2}}^{\pi - \phi_y^*} d\phi \cdot (-l \sin \psi \cos \phi) \cdot b + \int_{\psi_x^*}^{\frac{\pi}{2}} d\psi \int_{\pi - \phi_y^*}^{\pi - \phi_x^*} d\phi \cdot (-l \sin \psi \cos \phi) \cdot l \sin \psi \sin \phi \\
&+ \int_{\psi_x^*}^{\frac{\pi}{2}} d\psi \int_{\pi - \phi_x^*}^{\pi} d\phi \cdot a \cdot l \sin \psi \sin \phi \\
&= S^{(1)}(0, \psi_y^*) + S^{(2)}(\psi_y^*, \psi_x^*) + S^{(3)}\left(\psi_x^*, \frac{\pi}{2}\right).
\end{aligned} \tag{E.24}$$

In the above equations, we define and calculate a summation as

$$\begin{aligned}
S^{(3)}(\psi_x^*, \psi^*) &\equiv \int_{\psi_x^*}^{\psi^*} d\psi \int_0^{\phi_x^*} d\phi \cdot a \cdot l \sin \psi \sin \phi + \int_{\psi_x^*}^{\psi^*} d\psi \int_{\phi_x^*}^{\phi_y^*} d\phi \cdot l \sin \psi \cos \phi \cdot l \sin \psi \sin \phi \\
&+ \int_{\psi_x^*}^{\psi^*} d\psi \int_{\phi_y^*}^{\frac{\pi}{2}} d\phi \cdot l \sin \psi \cos \phi \cdot b \\
&+ \int_{\psi_x^*}^{\psi^*} d\psi \int_{\frac{\pi}{2}}^{\pi - \phi_y^*} d\phi \cdot (-l \sin \psi \cos \phi) \cdot b + \int_{\psi_x^*}^{\psi^*} d\psi \int_{\pi - \phi_y^*}^{\pi - \phi_x^*} d\phi \cdot (-l \sin \psi \cos \phi) \cdot l \sin \psi \sin \phi \\
&+ \int_{\psi_x^*}^{\psi^*} d\psi \int_{\pi - \phi_x^*}^{\pi} d\phi \cdot a \cdot l \sin \psi \sin \phi \\
&= 2la(\cos \psi_x^* - \cos \psi^*) - a^2(\psi^* - \psi_x^*) + 2lb(\cos \psi_x^* - \cos \psi^*) - b^2(\psi^* - \psi_x^*) \\
&- \left[\left(\frac{l^2}{2} \psi^* - \frac{l^2}{2} \sin \psi^* \cos \psi^* \right) - \left(\frac{l^2}{2} \psi_x^* - \frac{l^2}{2} \sin \psi_x^* \cos \psi_x^* \right) \right].
\end{aligned} \tag{E.25}$$

Thus we have

$$S^{(3)}\left(\psi_x^*, \frac{\pi}{2}\right) = 2la \cos \psi_x^* - a^2 \left(\frac{\pi}{2} - \psi_x^*\right) + 2lb \cos \psi_x^* - b^2 \left(\frac{\pi}{2} - \psi_x^*\right) - \left[\frac{\pi}{4}l^2 - \left(\frac{l^2}{2}\psi_x^* - \frac{la}{2}\cos \psi_x^*\right)\right], \quad (\text{E.26})$$

$$S^{(3)}(\psi_x^*, \psi_{xy}^*) = 2la(\cos \psi_x^* - \cos \psi_{xy}^*) - a^2(\psi_{xy}^* - \psi_x^*) + 2lb(\cos \psi_x^* - \cos \psi_{xy}^*) - b^2(\psi_{xy}^* - \psi_x^*) - \left[\left(\frac{l^2}{2}\psi_{xy}^* - \frac{lL}{2}\cos \psi_{xy}^*\right) - \left(\frac{l^2}{2}\psi_x^* - \frac{la}{2}\cos \psi_x^*\right)\right], \quad (\text{E.27})$$

in which we define

$$\psi_{xy}^* = \arcsin \frac{L}{l}. \quad (\text{E.28})$$

Then,

$$AB^{3D}(l, a, b|a < l \leq L) = \left[\frac{l^2}{2}\psi_x^* + \frac{3}{2}la \cos \psi_x^* - a^2 \left(\frac{\pi}{2} - \psi_x^*\right)\right] + \left[\frac{l^2}{2}\psi_y^* + \frac{3}{2}lb \cos \psi_y^* - b^2 \left(\frac{\pi}{2} - \psi_y^*\right)\right] - \frac{\pi}{4}l^2. \quad (\text{E.29})$$

We have

$$\begin{aligned} S_{\text{coll}}^{3D} &= bA^{3D}(l, a|a < l) + aB^{3D}(l, b|b < l) - AB^{3D}(l, a, b|a < l \leq L) \\ &= \left[2lb - 2lbF\left(\psi_x^*, \frac{\pi}{2}, \frac{a}{l}\right) + 2abG\left(\psi_x^*, \frac{\pi}{2}, \frac{a}{l}\right)\right] + \left[2la - 2laF\left(\psi_y^*, \frac{\pi}{2}, \frac{b}{l}\right) + 2abG\left(\psi_y^*, \frac{\pi}{2}, \frac{b}{l}\right)\right] \\ &\quad - \left[\frac{l^2}{2}\psi_x^* + \frac{3}{2}la \cos \psi_x^* - a^2 \left(\frac{\pi}{2} - \psi_x^*\right)\right] - \left[\frac{l^2}{2}\psi_y^* + \frac{3}{2}lb \cos \psi_y^* - b^2 \left(\frac{\pi}{2} - \psi_y^*\right)\right] + \frac{\pi}{4}l^2 \\ &= \left[2lb - 2lbF\left(\arcsin \frac{a}{l}, \frac{\pi}{2}, \frac{a}{l}\right) + 2abG\left(\arcsin \frac{a}{l}, \frac{\pi}{2}, \frac{a}{l}\right)\right] \\ &\quad + \left[2la - 2laF\left(\arcsin \frac{b}{l}, \frac{\pi}{2}, \frac{b}{l}\right) + 2abG\left(\arcsin \frac{b}{l}, \frac{\pi}{2}, \frac{b}{l}\right)\right] \\ &\quad - \left[\frac{l^2}{2}\arcsin \frac{a}{l} + \frac{3}{2}la\sqrt{1 - \frac{a^2}{l^2}} - a^2 \left(\frac{\pi}{2} - \arcsin \frac{a}{l}\right)\right] \\ &\quad - \left[\frac{l^2}{2}\arcsin \frac{b}{l} + \frac{3}{2}lb\sqrt{1 - \frac{b^2}{l^2}} - b^2 \left(\frac{\pi}{2} - \arcsin \frac{b}{l}\right)\right] + \frac{\pi}{4}l^2. \end{aligned} \quad (\text{E.30})$$

Then,

$$\begin{aligned} P^{3D}(l, a, b) &= \left[\frac{4}{\pi^2} \frac{l}{a} - \frac{4}{\pi^2} \frac{l}{a} F\left(\arcsin \frac{a}{l}, \frac{\pi}{2}, \frac{a}{l}\right) + \frac{4}{\pi^2} G\left(\arcsin \frac{a}{l}, \frac{\pi}{2}, \frac{a}{l}\right)\right] \\ &\quad + \left[\frac{4}{\pi^2} \frac{l}{b} - \frac{4}{\pi^2} \frac{l}{b} F\left(\arcsin \frac{b}{l}, \frac{\pi}{2}, \frac{b}{l}\right) + \frac{4}{\pi^2} G\left(\arcsin \frac{b}{l}, \frac{\pi}{2}, \frac{b}{l}\right)\right] \\ &\quad - \left[\frac{1}{\pi^2} \frac{l^2}{ab} \arcsin \frac{a}{l} + \frac{3}{\pi^2} \frac{l}{b} \sqrt{1 - \frac{a^2}{l^2}} - \frac{2}{\pi^2} \frac{a}{b} \left(\frac{\pi}{2} - \arcsin \frac{a}{l}\right)\right] \\ &\quad - \left[\frac{1}{\pi^2} \frac{l^2}{ab} \arcsin \frac{b}{l} + \frac{3}{\pi^2} \frac{l}{a} \sqrt{1 - \frac{b^2}{l^2}} - \frac{2}{\pi^2} \frac{b}{a} \left(\frac{\pi}{2} - \arcsin \frac{b}{l}\right)\right] + \frac{1}{2\pi} \frac{l^2}{ab}. \end{aligned} \quad (\text{E.31})$$

When $L < l$, we calculate the integral on ψ in $AB(l, a, b)$ in four ranges of $[0, \psi_y^*]$, $(\psi_y^*, \psi_x^*]$, $(\psi_y^*, \psi_{xy}^*]$, and $(\psi_{xy}^*, \pi/2]$

in a separate way. See Fig.5 (c) for a schematics. We write $AB^{3D}(l, a, b)$ when $L < l$ as $AB^{3D}(l, a, b|L < l)$, and have

$$\begin{aligned}
& AB^{3D}(l, a, b|L < l) \\
&= \int_0^{\psi_y^*} d\psi \int_0^{\frac{\pi}{2}} d\phi \cdot l \sin \psi \cos \phi \cdot l \sin \psi \sin \phi + \int_0^{\psi_y^*} d\psi \int_{\frac{\pi}{2}}^{\pi} d\phi \cdot (-l \sin \psi \cos \phi) \cdot l \sin \psi \sin \phi \\
&+ \int_{\psi_y^*}^{\psi_x^*} d\psi \int_0^{\phi_y^*} d\phi \cdot l \sin \psi \cos \phi \cdot l \sin \psi \sin \phi + \int_{\psi_y^*}^{\psi_x^*} d\psi \int_{\phi_y^*}^{\frac{\pi}{2}} d\phi \cdot l \sin \psi \cos \phi \cdot b \\
&+ \int_{\psi_y^*}^{\psi_x^*} d\psi \int_{\frac{\pi}{2}}^{\pi - \phi_y^*} d\phi \cdot (-l \sin \psi \cos \phi) \cdot b + \int_{\psi_y^*}^{\psi_x^*} d\psi \int_{\pi - \phi_y^*}^{\pi} d\phi \cdot (-l \sin \psi \cos \phi) \cdot l \sin \psi \sin \phi \\
&+ \int_{\psi_x^*}^{\psi_{xy}^*} d\psi \int_0^{\phi_x^*} d\phi \cdot a \cdot l \sin \psi \sin \phi + \int_{\psi_x^*}^{\psi_{xy}^*} d\psi \int_{\phi_x^*}^{\phi_y^*} d\phi \cdot l \sin \psi \cos \phi \cdot l \sin \psi \sin \phi \\
&+ \int_{\psi_x^*}^{\psi_{xy}^*} d\psi \int_{\phi_y^*}^{\frac{\pi}{2}} d\phi \cdot l \sin \psi \cos \phi \cdot b \\
&+ \int_{\psi_x^*}^{\psi_{xy}^*} d\psi \int_{\frac{\pi}{2}}^{\pi - \phi_y^*} d\phi \cdot (-l \sin \psi \cos \phi) \cdot b + \int_{\psi_x^*}^{\psi_{xy}^*} d\psi \int_{\pi - \phi_y^*}^{\pi - \phi_x^*} d\phi \cdot (-l \sin \psi \cos \phi) \cdot l \sin \psi \sin \phi \\
&+ \int_{\psi_x^*}^{\psi_{xy}^*} d\psi \int_{\pi - \phi_x^*}^{\pi} d\phi \cdot a \cdot l \sin \psi \sin \phi \\
&+ \int_{\frac{\pi}{2}}^{\frac{\pi}{2}} d\psi \int_0^{\phi_y^*} d\phi \cdot a \cdot l \sin \psi \sin \phi + \int_{\frac{\pi}{2}}^{\frac{\pi}{2}} d\psi \int_{\psi_{xy}^*}^{\phi_x^*} d\phi \cdot a \cdot b + \int_{\frac{\pi}{2}}^{\frac{\pi}{2}} d\psi \int_{\psi_{xy}^*}^{\frac{\pi}{2}} d\phi \cdot l \sin \psi \cos \phi \cdot b \\
&+ \int_{\frac{\pi}{2}}^{\frac{\pi}{2}} d\psi \int_{\frac{\pi}{2}}^{\pi - \phi_x^*} d\phi \cdot (-l \sin \psi \cos \phi) \cdot b + \int_{\frac{\pi}{2}}^{\frac{\pi}{2}} d\psi \int_{\psi_{xy}^*}^{\pi - \phi_x^*} d\phi \cdot a \cdot b + \int_{\frac{\pi}{2}}^{\frac{\pi}{2}} d\psi \int_{\pi - \phi_y^*}^{\pi} d\phi \cdot a \cdot l \sin \psi \sin \phi \\
&= S^{(1)}(0, \psi_y^*) + S^{(2)}(\psi_y^*, \psi_x^*) + S^{(3)}(\psi_x^*, \psi_{xy}^*) + S^{(4)}\left(\psi_{xy}^*, \frac{\pi}{2}\right). \tag{E.32}
\end{aligned}$$

In the above equations, we define and calculate a summation as

$$\begin{aligned}
S^{(4)}\left(\psi_{xy}^*, \frac{\pi}{2}\right) &= \int_{\psi_{xy}^*}^{\frac{\pi}{2}} d\psi \int_0^{\phi_y^*} d\phi \cdot a \cdot l \sin \psi \sin \phi + \int_{\psi_{xy}^*}^{\frac{\pi}{2}} d\psi \int_{\phi_y^*}^{\phi_x^*} d\phi \cdot a \cdot b + \int_{\psi_{xy}^*}^{\frac{\pi}{2}} d\psi \int_{\phi_x^*}^{\frac{\pi}{2}} d\phi \cdot l \sin \psi \cos \phi \cdot b \\
&+ \int_{\psi_{xy}^*}^{\frac{\pi}{2}} d\psi \int_{\frac{\pi}{2}}^{\pi - \phi_x^*} d\phi \cdot (-l \sin \psi \cos \phi) \cdot b + \int_{\psi_{xy}^*}^{\frac{\pi}{2}} d\psi \int_{\pi - \phi_x^*}^{\pi - \phi_y^*} d\phi \cdot a \cdot b + \int_{\psi_{xy}^*}^{\frac{\pi}{2}} d\psi \int_{\pi - \phi_y^*}^{\pi} d\phi \cdot a \cdot l \sin \psi \sin \phi \\
&= \left[2lb \cos \psi_{xy}^* - 2lbF\left(\psi_{xy}^*, \frac{\pi}{2}, \frac{a}{l}\right) + 2abG\left(\psi_{xy}^*, \frac{\pi}{2}, \frac{a}{l}\right) \right] \\
&+ \left[2la \cos \psi_{xy}^* - 2laF\left(\psi_{xy}^*, \frac{\pi}{2}, \frac{b}{l}\right) + 2abG\left(\psi_{xy}^*, \frac{\pi}{2}, \frac{b}{l}\right) \right] - ab\pi \left(\frac{\pi}{2} - \psi_{xy}^*\right). \tag{E.33}
\end{aligned}$$

Thus we have

$$\begin{aligned}
AB^{3D}(l, a, b|L < l) &= \left[-2lbF\left(\psi_{xy}^*, \frac{\pi}{2}, \frac{a}{l}\right) + 2abG\left(\psi_{xy}^*, \frac{\pi}{2}, \frac{a}{l}\right) \right] + \left[-2laF\left(\psi_{xy}^*, \frac{\pi}{2}, \frac{b}{l}\right) + 2abG\left(\psi_{xy}^*, \frac{\pi}{2}, \frac{b}{l}\right) \right] \\
&+ \left[\frac{l^2}{2} \psi_x^* + \frac{3}{2} la \cos \psi_x^* - a^2 \left(\frac{\pi}{2} - \psi_x^*\right) \right] + \left[\frac{l^2}{2} \psi_y^* + \frac{3}{2} lb \cos \psi_y^* - b^2 \left(\frac{\pi}{2} - \psi_y^*\right) \right] \\
&- \left[\frac{l^2}{2} \psi_{xy}^* - \frac{lL}{2} \cos \psi_{xy}^* - L^2 \left(\frac{\pi}{2} - \psi_{xy}^*\right) \right] - ab\pi \left(\frac{\pi}{2} - \psi_{xy}^*\right). \tag{E.34}
\end{aligned}$$

We have

$$\begin{aligned}
S_{\text{coll}}^{3D} &= bA^{3D}(l, a|a < l) + aB^{3D}(l, b|b < l) - AB^{3D}(l, a, b|L < l) \\
&= \left[2lb - 2lbF\left(\psi_x^*, \psi_{xy}^*, \frac{a}{l}\right) + 2abG\left(\psi_x^*, \psi_{xy}^*, \frac{a}{l}\right) \right] + \left[2la - 2laF\left(\psi_y^*, \psi_{xy}^*, \frac{b}{l}\right) + 2abG\left(\psi_y^*, \psi_{xy}^*, \frac{b}{l}\right) \right]
\end{aligned}$$

$$\begin{aligned}
& - \left[\frac{l^2}{2} \psi_x^* + \frac{3}{2} la \cos \psi_x^* - a^2 \left(\frac{\pi}{2} - \psi_x^* \right) \right] - \left[\frac{l^2}{2} \psi_y^* + \frac{3}{2} lb \cos \psi_y^* - b^2 \left(\frac{\pi}{2} - \psi_y^* \right) \right] \\
& + \left[\frac{l^2}{2} \psi_{xy}^* - \frac{lL}{2} \cos \psi_{xy}^* - L^2 \left(\frac{\pi}{2} - \psi_{xy}^* \right) \right] + ab\pi \left(\frac{\pi}{2} - \psi_{xy}^* \right) \\
& = \left[2lb - 2lbF \left(\arcsin \frac{a}{l}, \arcsin \frac{L}{l}, \frac{a}{l} \right) + 2abG \left(\arcsin \frac{a}{l}, \arcsin \frac{L}{l}, \frac{a}{l} \right) \right] \\
& + \left[2la - 2laF \left(\arcsin \frac{b}{l}, \arcsin \frac{L}{l}, \frac{b}{l} \right) + 2abG \left(\arcsin \frac{b}{l}, \arcsin \frac{L}{l}, \frac{b}{l} \right) \right] \\
& - \left[\frac{l^2}{2} \arcsin \frac{a}{l} + \frac{3}{2} la \sqrt{1 - \frac{a^2}{l^2}} - a^2 \left(\frac{\pi}{2} - \arcsin \frac{a}{l} \right) \right] \\
& - \left[\frac{l^2}{2} \arcsin \frac{b}{l} + \frac{3}{2} lb \sqrt{1 - \frac{b^2}{l^2}} - b^2 \left(\frac{\pi}{2} - \arcsin \frac{b}{l} \right) \right] \\
& + \left[\frac{l^2}{2} \arcsin \frac{L}{l} - \frac{lL}{2} \sqrt{1 - \frac{L^2}{l^2}} - L^2 \left(\frac{\pi}{2} - \arcsin \frac{L}{l} \right) \right] + ab\pi \left(\frac{\pi}{2} - \arcsin \frac{L}{l} \right). \tag{E.35}
\end{aligned}$$

Then,

$$\begin{aligned}
P^{3D}(l, a, b) &= \left[\frac{4}{\pi^2} \frac{l}{a} - \frac{4}{\pi^2} \frac{l}{a} F \left(\arcsin \frac{a}{l}, \arcsin \frac{L}{l}, \frac{a}{l} \right) + \frac{4}{\pi^2} G \left(\arcsin \frac{a}{l}, \arcsin \frac{L}{l}, \frac{a}{l} \right) \right] \\
&+ \left[\frac{4}{\pi^2} \frac{l}{b} - \frac{4}{\pi^2} \frac{l}{b} F \left(\arcsin \frac{b}{l}, \arcsin \frac{L}{l}, \frac{b}{l} \right) + \frac{4}{\pi^2} G \left(\arcsin \frac{b}{l}, \arcsin \frac{L}{l}, \frac{b}{l} \right) \right] \\
&- \left[\frac{1}{\pi^2} \frac{l^2}{ab} \arcsin \frac{a}{l} + \frac{3}{\pi^2} \frac{l}{b} \sqrt{1 - \frac{a^2}{l^2}} - \frac{2}{\pi^2} \frac{a}{b} \left(\frac{\pi}{2} - \arcsin \frac{a}{l} \right) \right] \\
&- \left[\frac{1}{\pi^2} \frac{l^2}{ab} \arcsin \frac{b}{l} + \frac{3}{\pi^2} \frac{l}{a} \sqrt{1 - \frac{b^2}{l^2}} - \frac{2}{\pi^2} \frac{b}{a} \left(\frac{\pi}{2} - \arcsin \frac{b}{l} \right) \right] \\
&+ \left[\frac{1}{\pi^2} \frac{l^2}{ab} \arcsin \frac{L}{l} - \frac{1}{\pi^2} \frac{lL}{ab} \sqrt{1 - \frac{L^2}{l^2}} - \frac{2}{\pi^2} \frac{L^2}{ab} \left(\frac{\pi}{2} - \arcsin \frac{L}{l} \right) \right] + \frac{2}{\pi} \left(\frac{\pi}{2} - \arcsin \frac{L}{l} \right). \tag{E.36}
\end{aligned}$$

XV. APPENDIX F: CONSISTENCY OF EQUATIONS IN THEORY OF BLNP WITH 3D NEEDLES

When $l = 0$, in the case of $l \leq b$, we have

$$P^{3D}(0, a, b) = 0, \tag{F.1}$$

which is intuitively correct.

When $l = b$, both the cases of $l \leq b$ and $b < l \leq a$ lead to

$$S_{\text{coll}}^{3D} = \left(2 - \frac{\pi}{4} \right) b^2 + 2ab. \tag{F.2}$$

When $l = a$, both the cases of $b < l \leq a$ and $a < l \leq L$ correspond to

$$\begin{aligned}
S_{\text{coll}}^{3D} &= 2ab + \left[2a^2 - 2a^2 F \left(\arcsin \frac{b}{a}, \frac{\pi}{2}, \frac{b}{a} \right) + 2abG \left(\arcsin \frac{b}{a}, \frac{\pi}{2}, \frac{b}{a} \right) \right] \\
&- \left[\frac{a^2}{2} \arcsin \frac{b}{a} + \frac{3}{2} ab \sqrt{1 - \frac{b^2}{a^2}} - b^2 \left(\frac{\pi}{2} - \arcsin \frac{b}{a} \right) \right]. \tag{F.3}
\end{aligned}$$

When $l = L$, both the cases of $a < l \leq L$ and $L < l$ result in

$$\begin{aligned} S_{\text{coll}}^{3\text{D}} = & \left[2bL - 2bLF \left(\arcsin \frac{a}{L}, \frac{\pi}{2}, \frac{a}{L} \right) + 2abG \left(\arcsin \frac{a}{L}, \frac{\pi}{2}, \frac{a}{L} \right) \right] \\ & + \left[2aL - 2aLF \left(\arcsin \frac{b}{L}, \frac{\pi}{2}, \frac{b}{L} \right) + 2abG \left(\arcsin \frac{b}{L}, \frac{\pi}{2}, \frac{b}{L} \right) \right] \\ & - \left[3ab - a^2 \left(\frac{\pi}{2} - \arcsin \frac{a}{L} \right) - b^2 \left(\frac{\pi}{2} - \arcsin \frac{b}{L} \right) \right]. \end{aligned} \quad (\text{F.4})$$

XVI. APPENDIX G: CASE OF INFINITELY LARGE l IN THEORY OF BLNP WITH 3D NEEDLES

For a general integral $H(a, b, t) \equiv \int_a^b d\psi h(\psi, t)$, if $a, b \rightarrow 0$ and both $h(a, t)$ and $h(b, t)$ are well-defined and finite, we have

$$H(a, b, t) \sim \frac{1}{2}(b - a)[h(a, t) + h(b, t)], \quad (\text{G.1})$$

based on the Trapezoidal rule in numerical integration methods [31]. Thus we have

$$\begin{aligned} lbF \left(\arcsin \frac{a}{l}, \arcsin \frac{L}{l}, \frac{a}{l} \right) & \sim lb \cdot \frac{1}{2} \left(\arcsin \frac{L}{l} - \arcsin \frac{a}{l} \right) \left[\sqrt{\frac{L^2}{l^2} - \frac{a^2}{l^2}} + \sqrt{\frac{a^2}{l^2} - \frac{a^2}{l^2}} \right] \\ & = \frac{1}{2}b^2 \left(\arcsin \frac{L}{l} - \arcsin \frac{a}{l} \right) \rightarrow 0, \end{aligned} \quad (\text{G.2})$$

$$laF \left(\arcsin \frac{b}{l}, \arcsin \frac{L}{l}, \frac{b}{l} \right) \sim \frac{1}{2}a^2 \left(\arcsin \frac{L}{l} - \arcsin \frac{b}{l} \right) \rightarrow 0. \quad (\text{G.3})$$

We further have

$$\begin{aligned} G \left(\arcsin \frac{a}{l}, \arcsin \frac{L}{l}, \frac{a}{l} \right) & \sim \frac{1}{2} \left(\arcsin \frac{L}{l} - \arcsin \frac{a}{l} \right) \left[\left(\frac{\pi}{2} - \arcsin \frac{a/l}{L/l} \right) + \left(\frac{\pi}{2} - \arcsin \frac{a/l}{a/l} \right) \right] \\ & = \frac{1}{2} \left(\arcsin \frac{L}{l} - \arcsin \frac{a}{l} \right) \left(\frac{\pi}{2} - \arcsin \frac{a}{L} \right) \rightarrow 0, \end{aligned} \quad (\text{G.4})$$

$$G \left(\arcsin \frac{b}{l}, \arcsin \frac{L}{l}, \frac{b}{l} \right) \sim \frac{1}{2} \left(\arcsin \frac{L}{l} - \arcsin \frac{b}{l} \right) \left(\frac{\pi}{2} - \arcsin \frac{b}{L} \right) \rightarrow 0. \quad (\text{G.5})$$

Summing up Eqs.(G.2)-(G.5), Eq.(E.35) reduces to

$$\begin{aligned} S_{\text{coll}}^{3\text{D}} = & [2lb - 2 \cdot 0 + 2ab \cdot 0] + [2la - 2 \cdot 0 + 2ab \cdot 0] \\ & - \left[\frac{l^2}{2} \cdot \frac{a}{l} + \frac{3}{2}la \cdot \sqrt{1-0} - a^2 \cdot \left(\frac{\pi}{2} - 0 \right) \right] - \left[\frac{l^2}{2} \cdot \frac{b}{l} + \frac{3}{2}lb \cdot \sqrt{1-0} - b^2 \cdot \left(\frac{\pi}{2} - 0 \right) \right] \\ & + \left[\frac{l^2}{2} \cdot \frac{L}{l} - \frac{lL}{2} \cdot \sqrt{1-0} - L^2 \cdot \left(\frac{\pi}{2} - 0 \right) \right] + ab\pi \cdot \left(\frac{\pi}{2} - 0 \right) \\ & = ab \frac{\pi^2}{2}. \end{aligned} \quad (\text{G.6})$$

Correspondingly, $P^{3\text{D}}(\infty, a, b) = 1$.

XVII. APPENDIX H: CALCULATION FOR THEORY OF BLNP WITH 3D SPHEROCYLINDERS

As Eqs.(E.2), (E.8), and (E.28) defined for the BLNP with 3D needles, we define their respective version for the BLNP with 3D spherocylinders as

$$\hat{\psi}_x^* = \arcsin \frac{a - \sigma}{l}, \quad (\text{H.1})$$

$$\hat{\psi}_y^* = \arcsin \frac{b - \sigma}{l}, \quad (\text{H.2})$$

$$\hat{\psi}_{xy}^* = \arcsin \frac{\hat{L}}{l}. \quad (\text{H.3})$$

When $l \leq b - \sigma$, with Eq. (54) we have

$$\begin{aligned}
S_{\text{coll}}^{3\text{D}} &= (b - \sigma)A^{3\text{D}}(l, a - \sigma | l \leq a - \sigma) + (a - \sigma)B^{3\text{D}}(l, b - \sigma | l \leq b - \sigma) \\
&\quad - AB^{3\text{D}}(l, a - \sigma, b - \sigma | l \leq b - \sigma) + (\sigma a + \sigma b - \sigma^2) \frac{\pi^2}{2} \\
&= 2l(b - \sigma) + 2l(a - \sigma) - \frac{\pi}{4}l^2 + (\sigma a + \sigma b - \sigma^2) \frac{\pi^2}{2}.
\end{aligned} \tag{H.4}$$

Then,

$$P^{3\text{D}}(l, \sigma, a, b) = \frac{4}{\pi^2} \frac{b - \sigma}{b} \frac{l}{a} + \frac{4}{\pi^2} \frac{a - \sigma}{a} \frac{l}{b} - \frac{1}{2\pi} \frac{l^2}{ab} + \left(\frac{\sigma}{a} + \frac{\sigma}{b} - \frac{\sigma^2}{ab} \right). \tag{H.5}$$

When $b - \sigma < l \leq a - \sigma$, we have

$$\begin{aligned}
S_{\text{coll}}^{3\text{D}} &= (b - \sigma)A^{3\text{D}}(l, a - \sigma | l \leq a - \sigma) + (a - \sigma)B^{3\text{D}}(l, b - \sigma | b - \sigma < l) \\
&\quad - AB^{3\text{D}}(l, a - \sigma, b - \sigma | b - \sigma < l \leq a - \sigma) + (\sigma a + \sigma b - \sigma^2) \frac{\pi^2}{2} \\
&= 2l(b - \sigma) + \left[2l(a - \sigma) - 2l(a - \sigma)F\left(\hat{\psi}_y^*, \frac{\pi}{2}, \frac{b - \sigma}{l}\right) + 2(a - \sigma)(b - \sigma)G\left(\hat{\psi}_y^*, \frac{\pi}{2}, \frac{b - \sigma}{l}\right) \right] \\
&\quad - \left[\frac{l^2}{2}\hat{\psi}_y^* + \frac{3}{2}l(b - \sigma)\cos\hat{\psi}_y^* - (b - \sigma)^2\left(\frac{\pi}{2} - \hat{\psi}_y^*\right) \right] + (\sigma a + \sigma b - \sigma^2) \frac{\pi^2}{2} \\
&= 2l(b - \sigma) + \left[2l(a - \sigma) - 2l(a - \sigma)F\left(\arcsin\frac{b - \sigma}{l}, \frac{\pi}{2}, \frac{b - \sigma}{l}\right) + 2(a - \sigma)(b - \sigma)G\left(\arcsin\frac{b - \sigma}{l}, \frac{\pi}{2}, \frac{b - \sigma}{l}\right) \right] \\
&\quad - \left[\frac{l^2}{2}\arcsin\frac{b - \sigma}{l} + \frac{3}{2}l(b - \sigma)\sqrt{1 - \frac{(b - \sigma)^2}{l^2}} - (b - \sigma)^2\left(\frac{\pi}{2} - \arcsin\frac{b - \sigma}{l}\right) \right] + (\sigma a + \sigma b - \sigma^2) \frac{\pi^2}{2}.
\end{aligned} \tag{H.6}$$

Then,

$$\begin{aligned}
P^{3\text{D}}(l, \sigma, a, b) &= \frac{4}{\pi^2} \frac{b - \sigma}{b} \frac{l}{a} + \left[\frac{4}{\pi^2} \frac{a - \sigma}{a} \frac{l}{b} - \frac{4}{\pi^2} \frac{a - \sigma}{a} \frac{l}{b} F\left(\arcsin\frac{b - \sigma}{l}, \frac{\pi}{2}, \frac{b - \sigma}{l}\right) + \frac{4}{\pi^2} \frac{a - \sigma}{a} \frac{b - \sigma}{b} G\left(\arcsin\frac{b - \sigma}{l}, \frac{\pi}{2}, \frac{b - \sigma}{l}\right) \right] \\
&\quad - \left[\frac{1}{\pi^2} \frac{l^2}{ab} \arcsin\frac{b - \sigma}{l} + \frac{3}{\pi^2} \frac{b - \sigma}{b} \frac{l}{a} \sqrt{1 - \frac{(b - \sigma)^2}{l^2}} - \frac{2}{\pi^2} \frac{(b - \sigma)^2}{ab} \left(\frac{\pi}{2} - \arcsin\frac{b - \sigma}{l}\right) \right] + \left(\frac{\sigma}{a} + \frac{\sigma}{b} - \frac{\sigma^2}{ab} \right).
\end{aligned} \tag{H.7}$$

When $a - \sigma < l \leq \hat{L}$, we have

$$\begin{aligned}
S_{\text{coll}}^{3\text{D}} &= (b - \sigma)A^{3\text{D}}(l, a - \sigma | a - \sigma < l) + (a - \sigma)B^{3\text{D}}(l, b - \sigma | b - \sigma < l) \\
&\quad - AB^{3\text{D}}(l, a - \sigma, b - \sigma | a - \sigma < l \leq \hat{L}) + (\sigma a + \sigma b - \sigma^2) \frac{\pi^2}{2} \\
&= \left[2l(b - \sigma) - 2l(b - \sigma)F\left(\hat{\psi}_x^*, \frac{\pi}{2}, \frac{a - \sigma}{l}\right) + 2(a - \sigma)(b - \sigma)G\left(\hat{\psi}_x^*, \frac{\pi}{2}, \frac{a - \sigma}{l}\right) \right] \\
&\quad + \left[2l(a - \sigma) - 2l(a - \sigma)F\left(\hat{\psi}_y^*, \frac{\pi}{2}, \frac{b - \sigma}{l}\right) + 2(a - \sigma)(b - \sigma)G\left(\hat{\psi}_y^*, \frac{\pi}{2}, \frac{b - \sigma}{l}\right) \right] \\
&\quad - \left[\frac{l^2}{2}\hat{\psi}_x^* + \frac{3}{2}l(a - \sigma)\cos\hat{\psi}_x^* - (a - \sigma)^2\left(\frac{\pi}{2} - \hat{\psi}_x^*\right) \right] \\
&\quad - \left[\frac{l^2}{2}\hat{\psi}_y^* + \frac{3}{2}l(b - \sigma)\cos\hat{\psi}_y^* - (b - \sigma)^2\left(\frac{\pi}{2} - \hat{\psi}_y^*\right) \right] \\
&\quad + \frac{\pi}{4}l^2 + (\sigma a + \sigma b - \sigma^2) \frac{\pi^2}{2} \\
&= \left[2l(b - \sigma) - 2l(b - \sigma)F\left(\arcsin\frac{a - \sigma}{l}, \frac{\pi}{2}, \frac{a - \sigma}{l}\right) + 2(a - \sigma)(b - \sigma)G\left(\arcsin\frac{a - \sigma}{l}, \frac{\pi}{2}, \frac{a - \sigma}{l}\right) \right]
\end{aligned}$$

$$\begin{aligned}
& + \left[2l(a-\sigma) - 2l(a-\sigma)F\left(\arcsin\frac{b-\sigma}{l}, \frac{\pi}{2}, \frac{b-\sigma}{l}\right) + 2(a-\sigma)(b-\sigma)G\left(\arcsin\frac{b-\sigma}{l}, \frac{\pi}{2}, \frac{b-\sigma}{l}\right) \right] \\
& - \left[\frac{l^2}{2} \arcsin\frac{a-\sigma}{l} + \frac{3}{2}l(a-\sigma)\sqrt{1-\frac{(a-\sigma)^2}{l^2}} - (a-\sigma)^2\left(\frac{\pi}{2} - \arcsin\frac{a-\sigma}{l}\right) \right] \\
& - \left[\frac{l^2}{2} \arcsin\frac{b-\sigma}{l} + \frac{3}{2}l(b-\sigma)\sqrt{1-\frac{(b-\sigma)^2}{l^2}} - (b-\sigma)^2\left(\frac{\pi}{2} - \arcsin\frac{b-\sigma}{l}\right) \right] \\
& + \frac{\pi}{4}l^2 + (\sigma a + \sigma b - \sigma^2)\frac{\pi^2}{2}.
\end{aligned} \tag{H.8}$$

Then,

$$\begin{aligned}
P^{3D}(l, \sigma, a, b) & = \left[\frac{4}{\pi^2} \frac{b-\sigma}{b} \frac{l}{a} - \frac{4}{\pi^2} \frac{b-\sigma}{b} \frac{l}{a} F\left(\arcsin\frac{a-\sigma}{l}, \frac{\pi}{2}, \frac{a-\sigma}{l}\right) + \frac{4}{\pi^2} \frac{a-\sigma}{a} \frac{b-\sigma}{b} G\left(\arcsin\frac{a-\sigma}{l}, \frac{\pi}{2}, \frac{a-\sigma}{l}\right) \right] \\
& + \left[\frac{4}{\pi^2} \frac{a-\sigma}{a} \frac{l}{b} - \frac{4}{\pi^2} \frac{a-\sigma}{a} \frac{l}{b} F\left(\arcsin\frac{b-\sigma}{l}, \frac{\pi}{2}, \frac{b-\sigma}{l}\right) + \frac{4}{\pi^2} \frac{a-\sigma}{a} \frac{b-\sigma}{b} G\left(\arcsin\frac{b-\sigma}{l}, \frac{\pi}{2}, \frac{b-\sigma}{l}\right) \right] \\
& - \left[\frac{1}{\pi^2} \frac{l^2}{ab} \arcsin\frac{a-\sigma}{l} + \frac{3}{\pi^2} \frac{a-\sigma}{a} \frac{l}{b} \sqrt{1-\frac{(a-\sigma)^2}{l^2}} - \frac{2}{\pi^2} \frac{(a-\sigma)^2}{ab} \left(\frac{\pi}{2} - \arcsin\frac{a-\sigma}{l}\right) \right] \\
& - \left[\frac{1}{\pi^2} \frac{l^2}{ab} \arcsin\frac{b-\sigma}{l} + \frac{3}{\pi^2} \frac{b-\sigma}{b} \frac{l}{a} \sqrt{1-\frac{(b-\sigma)^2}{l^2}} - \frac{2}{\pi^2} \frac{(b-\sigma)^2}{ab} \left(\frac{\pi}{2} - \arcsin\frac{b-\sigma}{l}\right) \right] \\
& + \frac{1}{2\pi} \frac{l^2}{ab} + \left(\frac{\sigma}{a} + \frac{\sigma}{b} - \frac{\sigma^2}{ab}\right).
\end{aligned} \tag{H.9}$$

When $\hat{L} < l$, we have

$$\begin{aligned}
S_{\text{coll}}^{3D} & = (b-\sigma)A^{3D}(l, a-\sigma|a-\sigma < l) + (a-\sigma)B^{3D}(l, b-\sigma|b-\sigma < l) \\
& - AB^{3D}(l, a-\sigma, b-\sigma|\hat{L} < l) + (\sigma a + \sigma b - \sigma^2)\frac{\pi^2}{2} \\
& = \left[2l(b-\sigma) - 2l(b-\sigma)F\left(\hat{\psi}_x^*, \hat{\psi}_{xy}^*, \frac{a-\sigma}{l}\right) + 2(a-\sigma)(b-\sigma)G\left(\hat{\psi}_x^*, \hat{\psi}_{xy}^*, \frac{a-\sigma}{l}\right) \right] \\
& + \left[2l(a-\sigma) - 2l(a-\sigma)F\left(\hat{\psi}_y^*, \hat{\psi}_{xy}^*, \frac{b-\sigma}{l}\right) + 2(a-\sigma)(b-\sigma)G\left(\hat{\psi}_y^*, \hat{\psi}_{xy}^*, \frac{b-\sigma}{l}\right) \right] \\
& - \left[\frac{l^2}{2} \hat{\psi}_x^* + \frac{3}{2}l(a-\sigma)\cos\hat{\psi}_x^* - (a-\sigma)^2\left(\frac{\pi}{2} - \hat{\psi}_x^*\right) \right] \\
& - \left[\frac{l^2}{2} \hat{\psi}_y^* + \frac{3}{2}l(b-\sigma)\cos\hat{\psi}_y^* - (b-\sigma)^2\left(\frac{\pi}{2} - \hat{\psi}_y^*\right) \right] \\
& + \left[\frac{l^2}{2} \hat{\psi}_{xy}^* - \frac{l\hat{L}}{2} \cos\hat{\psi}_{xy}^* - \hat{L}^2\left(\frac{\pi}{2} - \hat{\psi}_{xy}^*\right) \right] \\
& + (a-\sigma)(b-\sigma)\pi\left(\frac{\pi}{2} - \hat{\psi}_{xy}^*\right) + (\sigma a + \sigma b - \sigma^2)\frac{\pi^2}{2} \\
& = \left[2l(b-\sigma) - 2l(b-\sigma)F\left(\arcsin\frac{a-\sigma}{l}, \arcsin\frac{\hat{L}}{l}, \frac{a-\sigma}{l}\right) + 2(a-\sigma)(b-\sigma)G\left(\arcsin\frac{a-\sigma}{l}, \arcsin\frac{\hat{L}}{l}, \frac{a-\sigma}{l}\right) \right] \\
& + \left[2l(a-\sigma) - 2l(a-\sigma)F\left(\arcsin\frac{b-\sigma}{l}, \arcsin\frac{\hat{L}}{l}, \frac{b-\sigma}{l}\right) + 2(a-\sigma)(b-\sigma)G\left(\arcsin\frac{b-\sigma}{l}, \arcsin\frac{\hat{L}}{l}, \frac{b-\sigma}{l}\right) \right] \\
& - \left[\frac{l^2}{2} \arcsin\frac{a-\sigma}{l} + \frac{3}{2}l(a-\sigma)\sqrt{1-\frac{(a-\sigma)^2}{l^2}} - (a-\sigma)^2\left(\frac{\pi}{2} - \arcsin\frac{a-\sigma}{l}\right) \right] \\
& - \left[\frac{l^2}{2} \arcsin\frac{b-\sigma}{l} + \frac{3}{2}l(b-\sigma)\sqrt{1-\frac{(b-\sigma)^2}{l^2}} - (b-\sigma)^2\left(\frac{\pi}{2} - \arcsin\frac{b-\sigma}{l}\right) \right]
\end{aligned}$$

$$\begin{aligned}
& + \left[\frac{l^2}{2} \arcsin \frac{\hat{L}}{l} - \frac{l\hat{L}}{2} \sqrt{1 - \frac{\hat{L}^2}{l^2}} - \hat{L}^2 \left(\frac{\pi}{2} - \arcsin \frac{\hat{L}}{l} \right) \right] \\
& + (a - \sigma)(b - \sigma)\pi \left(\frac{\pi}{2} - \arcsin \frac{\hat{L}}{l} \right) + (\sigma a + \sigma b - \sigma^2) \frac{\pi^2}{2}.
\end{aligned} \tag{H.10}$$

Then,

$$\begin{aligned}
& P^{3D}(l, \sigma, a, b) \\
& = \left[\frac{4}{\pi^2} \frac{b - \sigma}{b} \frac{l}{a} - \frac{4}{\pi^2} \frac{b - \sigma}{b} \frac{l}{a} F \left(\arcsin \frac{a - \sigma}{l}, \arcsin \frac{\hat{L}}{l}, \frac{a - \sigma}{l} \right) + \frac{4}{\pi^2} \frac{a - \sigma}{a} \frac{b - \sigma}{b} G \left(\arcsin \frac{a - \sigma}{l}, \arcsin \frac{\hat{L}}{l}, \frac{a - \sigma}{l} \right) \right] \\
& + \left[\frac{4}{\pi^2} \frac{a - \sigma}{a} \frac{l}{b} - \frac{4}{\pi^2} \frac{a - \sigma}{a} \frac{l}{b} F \left(\arcsin \frac{b - \sigma}{l}, \arcsin \frac{\hat{L}}{l}, \frac{b - \sigma}{l} \right) + \frac{4}{\pi^2} \frac{a - \sigma}{a} \frac{b - \sigma}{b} G \left(\arcsin \frac{b - \sigma}{l}, \arcsin \frac{\hat{L}}{l}, \frac{b - \sigma}{l} \right) \right] \\
& - \left[\frac{1}{\pi^2} \frac{l^2}{ab} \arcsin \frac{a - \sigma}{l} + \frac{3}{\pi^2} \frac{a - \sigma}{a} \frac{l}{b} \sqrt{1 - \frac{(a - \sigma)^2}{l^2}} - \frac{2}{\pi^2} \frac{(a - \sigma)^2}{ab} \left(\frac{\pi}{2} - \arcsin \frac{a - \sigma}{l} \right) \right] \\
& - \left[\frac{1}{\pi^2} \frac{l^2}{ab} \arcsin \frac{b - \sigma}{l} + \frac{3}{\pi^2} \frac{b - \sigma}{b} \frac{l}{a} \sqrt{1 - \frac{(b - \sigma)^2}{l^2}} - \frac{2}{\pi^2} \frac{(b - \sigma)^2}{ab} \left(\frac{\pi}{2} - \arcsin \frac{b - \sigma}{l} \right) \right] \\
& + \left[\frac{1}{\pi^2} \frac{l^2}{ab} \arcsin \frac{\hat{L}}{l} - \frac{1}{\pi^2} \frac{l\hat{L}}{ab} \sqrt{1 - \frac{\hat{L}^2}{l^2}} - \frac{2}{\pi^2} \frac{\hat{L}^2}{ab} \left(\frac{\pi}{2} - \arcsin \frac{\hat{L}}{l} \right) \right] \\
& + \frac{2}{\pi} \frac{a - \sigma}{a} \frac{b - \sigma}{b} \left(\frac{\pi}{2} - \arcsin \frac{\hat{L}}{l} \right) + \left(\frac{\sigma}{a} + \frac{\sigma}{b} - \frac{\sigma^2}{ab} \right).
\end{aligned} \tag{H.11}$$

XVIII. APPENDIX I: CONSISTENCY OF EQUATIONS IN THEORY OF BLNP WITH 3D SPHEROCYLINDERS

When $l = 0$, based on the case of $l \leq b$, we have

$$S_{\text{coll}}^{3D} = (\sigma a + \sigma b - \sigma^2) \frac{\pi^2}{2}, \tag{I.1}$$

which is simply S_{coll} in Eq. (D.1) for the problem of 2D spherocylinders with $l = 0$, multiplying by the range of the new degree of freedom ψ , or $\pi/2$.

When $l = b - \sigma$, both the cases of $l \leq b - \sigma$ and $b - \sigma < l \leq a - \sigma$ reduce to

$$S_{\text{coll}}^{3D} = \left(2 - \frac{\pi}{4} \right) (b - \sigma)^2 + 2(a - \sigma)(b - \sigma) + (\sigma a + \sigma b - \sigma^2) \frac{\pi^2}{2}. \tag{I.2}$$

When $l = a - \sigma$, both the cases of $b - \sigma < l \leq a - \sigma$ and $a - \sigma < l \leq \hat{L}$ correspond to

$$\begin{aligned}
& S_{\text{coll}}^{3D} = 2(a - \sigma)(b - \sigma) \\
& + \left[2(a - \sigma)^2 - 2(a - \sigma)^2 F \left(\arcsin \frac{b - \sigma}{a - \sigma}, \frac{\pi}{2}, \frac{b - \sigma}{a - \sigma} \right) + 2(a - \sigma)(b - \sigma) G \left(\arcsin \frac{b - \sigma}{a - \sigma}, \frac{\pi}{2}, \frac{b - \sigma}{a - \sigma} \right) \right] \\
& - \left[\frac{(a - \sigma)^2}{2} \arcsin \frac{b - \sigma}{a - \sigma} + \frac{3}{2} (a - \sigma)(b - \sigma) \sqrt{1 - \frac{(b - \sigma)^2}{(a - \sigma)^2}} - (b - \sigma)^2 \left(\frac{\pi}{2} - \arcsin \frac{b - \sigma}{a - \sigma} \right) \right] \\
& + (\sigma a + \sigma b - \sigma^2) \frac{\pi^2}{2}.
\end{aligned} \tag{I.3}$$

When $l = \hat{L}$, both the cases of $a - \sigma < l \leq \hat{L}$ and $\hat{L} < l$ result in

$$\begin{aligned}
S_{\text{coll}}^{3\text{D}} = & \left[2\hat{L}(b - \sigma) - 2\hat{L}(b - \sigma)F\left(\arcsin \frac{a - \sigma}{\hat{L}}, \frac{\pi}{2}, \frac{a - \sigma}{\hat{L}}\right) + 2(a - \sigma)(b - \sigma)G\left(\arcsin \frac{a - \sigma}{\hat{L}}, \frac{\pi}{2}, \frac{a - \sigma}{\hat{L}}\right) \right] \\
& + \left[2\hat{L}(a - \sigma) - 2\hat{L}(a - \sigma)F\left(\arcsin \frac{b - \sigma}{\hat{L}}, \frac{\pi}{2}, \frac{b - \sigma}{\hat{L}}\right) + 2(a - \sigma)(b - \sigma)G\left(\arcsin \frac{b - \sigma}{\hat{L}}, \frac{\pi}{2}, \frac{b - \sigma}{\hat{L}}\right) \right] \\
& - \left[3(a - \sigma)(b - \sigma) - (a - \sigma)^2 \left(\frac{\pi}{2} - \arcsin \frac{a - \sigma}{\hat{L}}\right) - (b - \sigma)^2 \left(\frac{\pi}{2} - \arcsin \frac{b - \sigma}{\hat{L}}\right) \right] \\
& + (\sigma a + \sigma b - \sigma^2) \frac{\pi^2}{2}.
\end{aligned} \tag{I.4}$$

XIX. APPENDIX J: CASE OF INFINITELY LARGE l IN THEORY OF BLNP WITH 3D SPHEROCYLINDERS

With Eqs.(G.2)-(G.5) and substituting (a, b, L) with $(a - \sigma, b - \sigma, \hat{L})$ respectively, we have

$$l(b - \sigma)F\left(\arcsin \frac{a - \sigma}{l}, \arcsin \frac{\hat{L}}{l}, \frac{a - \sigma}{l}\right) \sim \frac{1}{2}(b - \sigma)^2 \left(\arcsin \frac{\hat{L}}{l} - \arcsin \frac{a - \sigma}{l}\right) \rightarrow 0, \tag{J.1}$$

$$l(a - \sigma)F\left(\arcsin \frac{b - \sigma}{l}, \arcsin \frac{\hat{L}}{l}, \frac{b - \sigma}{l}\right) \sim \frac{1}{2}(a - \sigma)^2 \left(\arcsin \frac{\hat{L}}{l} - \arcsin \frac{b - \sigma}{l}\right) \rightarrow 0, \tag{J.2}$$

$$G\left(\arcsin \frac{a - \sigma}{l}, \arcsin \frac{\hat{L}}{l}, \frac{a - \sigma}{l}\right) \sim \frac{1}{2} \left(\arcsin \frac{\hat{L}}{l} - \arcsin \frac{a - \sigma}{l}\right) \left(\frac{\pi}{2} - \arcsin \frac{a - \sigma}{\hat{L}}\right) \rightarrow 0, \tag{J.3}$$

$$G\left(\arcsin \frac{b - \sigma}{l}, \arcsin \frac{\hat{L}}{l}, \frac{b - \sigma}{l}\right) \sim \frac{1}{2} \left(\arcsin \frac{\hat{L}}{l} - \arcsin \frac{b - \sigma}{l}\right) \left(\frac{\pi}{2} - \arcsin \frac{b - \sigma}{\hat{L}}\right) \rightarrow 0. \tag{J.4}$$

Thus Eq.(H.10) reduces to

$$\begin{aligned}
S_{\text{coll}}^{3\text{D}} = & [2l(b - \sigma) - 2 \cdot 0 + 2(a - \sigma)(b - \sigma) \cdot 0] \\
& + [2l(a - \sigma) - 2 \cdot 0 + 2(a - \sigma)(b - \sigma) \cdot 0] \\
& - \left[\frac{l^2}{2} \cdot \frac{a - \sigma}{l} + \frac{3}{2}l(a - \sigma) \cdot \sqrt{1 - 0} - (a - \sigma)^2 \cdot \left(\frac{\pi}{2} - 0\right) \right] \\
& - \left[\frac{l^2}{2} \cdot \frac{b - \sigma}{l} + \frac{3}{2}l(b - \sigma) \cdot \sqrt{1 - 0} - (b - \sigma)^2 \cdot \left(\frac{\pi}{2} - 0\right) \right] \\
& + \left[\frac{l^2}{2} \cdot \frac{\hat{L}}{l} - \frac{l\hat{L}}{2} \cdot \sqrt{1 - 0} - \hat{L}^2 \cdot \left(\frac{\pi}{2} - 0\right) \right] \\
& + (a - \sigma)(b - \sigma)\pi \cdot \left(\frac{\pi}{2} - 0\right) + (\sigma a + \sigma b - \sigma^2) \frac{\pi^2}{2} \\
= & ab \frac{\pi^2}{2}.
\end{aligned} \tag{J.5}$$

Equivalently, $P^{3\text{D}}(\infty, \sigma, a, b) = 1$.

-
- [1] C. Tien, B. V. Ramarao, *Granular Filtration of Aerosols and Hydrosols*, Second Edition (Elsevier, Oxford, 2007).
[2] H. M. Jaeger, S. R. Nagel, R. P. Behringer, Granular solids, liquids, and gases, *Rev. Modern Phys.* 68 (1996) 1259–1273.
[3] S. Redner, S. Datta, Clogging Time of a Filter, *Phys. Rev. Lett.* 84 (2000) 6018–6021.
[4] K. To, P.-Y. Lai, H. K. Pak, Jamming of Granular Flow in a Two-Dimensional Hopper, *Phys. Rev. Lett.* 86 (2001) 71–74.
[5] N. Roussel, T. L. H. Nguyen, P. Coussot, General Probabilistic Approach to the Filtration Process, *Phys. Rev. Lett.* 98 (2007) 114502.

- [6] A. Gabrielli, J. Talbot, P. Viot, Non-Markovian Models of Blocking in Concurrent and Countercurrent Flows, *Phys. Rev. Lett.* 110 (2013) 170601.
- [7] G. Gerber, S. Rodts, P. Aïmeidieu, P. Faure, P. Coussot, Particle-Size-Exclusion Clogging Regimes in Porous Media, *Phys. Rev. Lett.* 120 (2018) 148001.
- [8] Z. E. Dell, S. V. Franklin, The Buffon-Laplace needle problem in three dimensions, *J. Stat. Mech.* (2009) P09010.
- [9] P.-S. Laplace, *Théorie analytique des probabilités* (Veuve Courcier, Paris, 1812).
- [10] P.-S. Laplace, *Théorie analytique des probabilités*, Third Revised Edition (Veuve Courcier, Paris, 1820).
- [11] G.-L. Buffon, Essai d'arithmétique morale, Histoire naturelle, générale et particulière, Supplément 4 (1777) 46–123.
- [12] A. Rényi, On a one-dimensional problem concerning random space-filling, *Publ. Math. Inst. Hung. Acad. Sci.* 3 (1958) 109–127.
- [13] R. D. Vigil, R. M. Ziff, Kinetics of random sequential adsorption of rectangles and line segments, *J. Chem. Phys.* 93 (1990) 8270–8272.
- [14] N. M. Švrakić, M. Henkel, Kinetics of irreversible deposition of mixtures, *J. Phys. I* 1 (1991) 791–795.
- [15] J. W. Evans, Random and cooperative sequential adsorption, *Rev. Modern Phys.* 65 (1993) 1281–1329.
- [16] L. Böttcher, A Random-Line-Graph Approach to Overlapping Line Segments, *J. Comp. Netw.* 8 (2020) cnaa029.
- [17] J. V. Uspensky, *Introduction to Mathematical Probability* (McGraw-Hill, New York, 1937).
- [18] P. Diaconis, Buffon's Problem with a Long Needle, *J. Appl. Probab.* 13 (1976) 614–618.
- [19] A. Arkhipov, L. Mendo, On the number of tiles visited by a line segment on a rectangular grid, *Mathematika* 69 (2023) 1242–1281.
- [20] E. Barbier, Note sur le problème de l'aiguille et le jeu du joint couvert, *Journal de mathématiques pures et appliquées* 2e série 5 (1860) 273–286.
- [21] J. F. Ramaley, Buffon's Noodle Problem, *Am. Math. Mon.* 76 (1969) 916–918.
- [22] I. G. Johannesen, The Buffon Needle Problem Revisited in a Pedagogical Perspective, *Math. J.* 11 (2009) 284–299.
- [23] U. Bäsel, Buffon's problem with a pivot needle, *Elem. Math.* 70 (2015) 67–70.
- [24] C. F. Chung, Application of the Buffon Needle Problem and its Extensions to Parallel-Line Search Sampling Scheme, *Math. Geosci.* 12 (1981) 371–390.
- [25] S. Zhang, The exact power law for Buffon's needle landing near some random Cantor sets, *Rev. Mat. Iberoam.* 36 (2020) 537–548.
- [26] D. Vardakis, A. Volberg, The Buffon's needle problem for random planar disk-like Cantor sets, *J. Math. Anal. Appl.* 529 (2024) 127622.
- [27] C. Godréche, The Buffon needle problem for Lévy distributed spacings and renewal theory, *J. Stat. Mech.* (2022) 013203.
- [28] A. Duma, M. Stoka, Hitting probabilities for random ellipses and ellipsoids, *J. Appl. Probab.* 30 (1993) 971–974.
- [29] L. Pournin, M. Weber, M. Tsukahara, J.-A. Ferrez, M. Ramaioli, Th. M. Lieblich, Three-dimensional distinct element simulation of spherocylinder crystallization, *Granul. Matter* 7 (2005) 119–126.
- [30] D. P. Landau, K. Binder. *A Guide to Monte Carlo Simulations in Statistical Physics*, Fourth Edition (Cambridge University Press, Cambridge, 2015).
- [31] W. H. Press, S. A. Teukolsky, W. T. Vetterling, B. P. Flannery, *Numerical Recipes: The Art of Scientific Computing*, Third Edition (Cambridge University Press, Cambridge, 2007).
- [32] M. Scheffer, *Critical Transitions in Nature and Society* (Princeton University Press, Princeton, 2009).